nature portfolio

https://doi.org/10.1038/s44160-022-00071-y

Supplementary information

Constructing ambivalent imidazopyridinium-linked covalent organic frameworks

In the format provided by the authors and unedited

Constructing Ambivalent Imidazopyridinium-Linked Covalent Organic Frameworks

Xing Li#,[1] Kun Zhang#,[1] Gang Wang,[2] Yijia Yuan,[1] Gaolei Zhan,[1] Tanmay Ghosh,[3, 4] Walter P.D. Wong,[1] Fangzheng Chen,[1] Hai-Sen Xu,[1] Utkur Mirsaidov,[3, 4] Keyu Xie,[5] Junhao Lin,[2]* Kian Ping Loh[1]*

[1]Department of Chemistry, National University of Singapore, 3 Science Drive 3, Singapore 117543, Singapore.
[2]Department of Physics and Shenzhen Key Laboratory of Advanced Quantum Functional Materials and Devices, Southern University of Science and Technology, Shenzhen 518055, China.
[3]Department of Physics, National University of Singapore, 2 Science Drive 3, Singapore 117551, Singapore.
[4]Centre for BioImaging Sciences, Department of Biological Sciences, National University of Singapore, 14 Science Drive 4, Singapore 117557, Singapore.
[5]State Key Laboratory of Solidification Processing, Center for Nano Energy Materials, Northwestern Polytechnical University and Shaanxi Joint Laboratory of Graphene (NPU), Xi'an 710072, P.R. China.
[#]These authors contributed equally to this work.

*Corresponding Author: linjh@sustech.edu.cn; chmlohkp@nus.edu.sg

Contents

General Information

Materials and Methods

All commercially available chemicals and solvents were purchased from Sigma Aldrich and TCI, and used as received without further purification.

Nuclear Magnetic Resonance spectroscopy (NMR):
NMR spectra were collected on a Bruker AMX400 (400 MHz) spectrometer. Chemical shifts were reported in parts per million (ppm). Residual solvent peak was used as an internal reference.

Solid-state NMR:
Solid-state NMR experiments were performed on a 9 T Bruker Advance Neo 400 MHz wide-bore spectrometer with an Agilent 5.0 mm T3 probe. Samples were packed in a 4 mm zirconium oxide rotor. 1D ^{1}H-^{13}C CP-MAS NMR spectra were collected with 10 kHz MAS spinning frequency and the variable temperature was kept at 296 K.

High resolution mass spectra (HRMS):
All HRMS were recorded on a Finnigan/MAT 95XL-T spectrometer in ESI mode.

Fourier transform infrared (FT-IR):
All FT-IR spectra were recorded on a Bruker vertex 80v spectrometer.

Elemental analysis:
Elemental analysis was performed on Elementar vario MICRO cube for C, H, N and S.

Melting point:
Melting point data were recorded on Buchi Melting Point M-560 at a ramp rate of 5 °C min^{-1}.

Thermogravimetric analysis (TGA):
TGA was recorded on a TGA 500 thermogravimetric analyser by heating the samples at a ramp rate of 10 °C min^{-1} to 800 °C in a nitrogen atmosphere.

Powder X-ray diffraction (PXRD) measurements:
PXRD experiments were performed on Wide-angle X-ray diffraction (XRD) patterns and collected on a Bruker D8 Focus Powder X-ray diffractometer using Cu Kα radiation (40 kV, 40 mA) at room temperature. The FWHM of (110) peaks were estimated using the Bruker software diffraceva-v5.1, and the corresponding crystallite sizes were calculated using the Scherrer equation in the software.

Gas sorption measurements:
Gas sorption analysis were performed on Quantachrome Instruments Autosorb-iQ (Boynton Beach, Florida USA) with extra-high pure gases. The samples were activated and outgassed at 120 ºC for 8 h before measurement. The Brunauer-Emmett-Teller (BET) surface area and total pore volume were calculated from the N_2 sorption isotherms at 77 K, and the pore size distribution was calculated based on the N_2 sorption isotherm by using Non-Local Density Functional Theory (NL-DFT, a carbon model containing slit/cylindrical pore) model in the Quantachrome ASiQwin 5.0 software package.

Scanning electron microscopy (SEM):
SEM images were taken on a JEOL JSM-6701F Field-Emission microscope.

Transmission electron microscopy (TEM):
The low-dose TEM images were acquired on a 300 kV Thermo Fisher Titan TEM equipped (Thermo Fisher Scientific, Hillsboro, OR, USA) with a Gatan K2-IS direct electron detection camera (Gatan, Pleasanton, CA, USA). The camera was operated in electron counting mode and the imaging electron flux was kept to 20-70 $e^{-}/(Å^2 \cdot s)$.

Sample preparation and Cryo-TEM characterization:
The crystalline COF powder was dispersed in ethanol and centrifuged at 6000 rpm after ultrasonication for 30 min at room temperature to obtain the supernatant, which was then dropped on Quantifoil R 0.6/1

holey carbon grid for further TEM investigation. An aberration-corrected Titan Krios G3 cryogenic TEM operated at 300 kV was used to characterize the COF specimens at liquid nitrogen temperature. All TEM images were acquired by a direct-detection electron-counting camera Falcon 3 controlled by EPU and Velox software (Thermo Fisher Scientific Ltd.), and the measured electron dose for HRTEM was around 50 e^{-} $Å^{-2}$.

X-ray photoelectron spectroscopy (XPS):
Chemical compositions of electrodes before and after cycles were analyzed by X-ray photoelectron spectroscopy (XPS, Kratos XSAM 800, with Al Kα radiation source (12 mA, 12 kV)).

Atomic force microscopy (AFM):
The morphology of thin films was investigated by a ScanAsyst model AFM (Bruker Dimension Icon with Nanoscope V controller) under ambient conditions. The probe consisted of a sharp silicon tip (SCANASYST-AIR; thickness: 2.5–8.0 µm, length: 115 µm, width: 25 µm; resonance frequency: 70 kHz; spring constant: 0.4 N m^{-1}) attached to a silicon nitride cantilever. Scan frequencies of 0.6 Hz for good imaging conditions. AFM images were analysed with the software WSXM.

For the high-resolution AFM, Tapping-mode AFM imaging was performed under ambient conditions immediately after sample preparation using an Asylum Cypher ES AFM (Oxford Instruments-Asylum Research, Santa Barbara, USA). To achieve ultra-high-resolution images we use high-frequency Arrow UHF probes (NanoWorld AG, Neuchâtel, Switzerland) driven at the first eigenmode, corresponding to resonant frequency of ~1.5 MHz. The amplitude sensitivity (15 nm/V) was estimated using the thermal method as implemented in GetReal calibration procedure (Oxford Instruments-Asylum Research). The scanning parameters were optimized for each AFM scan. Scan rate 4.88 Hz, 512 x 512 px, setpoint 9.5 mV, oscillation amplitudes of 3–9 nm (200–600 mV for Arrow UHF probes).

Structural modelling method:
Molecular modelling and Pawley refinement were conducted using Reflex, a software package for crystal determination using Powder XRD pattern, implemented in BIOVIA Materials Studio modelling version, 2016 (Dassault System)[1]. For COFs structural determination, the lattice model was optimized using the Materials Studio Forcite molecular dynamics module under ultra-fine, Universal force fields, Ewald summations condition. Then Pawley refinement was performed to optimize the lattice parameters until the R_{wp} value converged. The pseudo-Voigt profile function and Berrar–Baldinozzi function were used for whole profile fitting and asymmetry correction respectively during the refinement process.

Synthetic Procedures

Synthetic procedures of COF building units and model compound

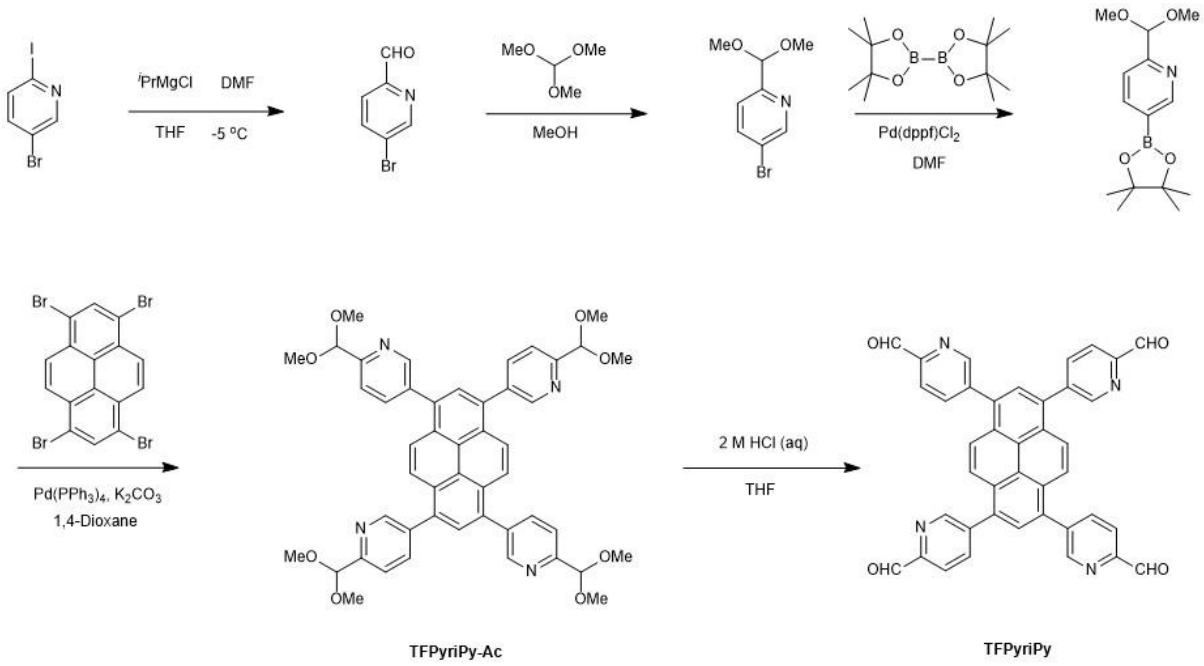

Supplementary Fig. 1 | Synthesis of tetratopic picolinaldehyde building units.

5-bromopicolinaldehyde: To a solution of 2-iodo-5-brompyridine (10 g, 35.2 mmol) in anhydrous THF (100 ml) at −5 °C was added ^{i}PrMgCl (19.35 ml, 2 M in THF). The mixture was stirred at −5 °C for 1 h and then added with anhydrous DMF (4.1 ml, 53.2 mmol) dropwisely. The mixture was stirred for a further 0.5 h at −5 °C and then allowed to warm to room temperature. HCl (16 ml, 2 M aq, 32 mmol) was added dropwisely and the mixture was stirred for another 0.5 h. The acidic solution was neutralized by addition of NaOH at 0 °C. The mixture was then extracted with DCM (4 × 100 ml), and the organic layer was combined, dried over Na_2SO_4 and evaporated *via* vacuum to give an off-white solid. The crude product was recrystallized in CH_2Cl_2/Hexane to give a white crystalline solid (5.79 g, 88%). ^{1}H NMR (400 MHz, $CDCl_3$) δ 10.04 (d, *J* = 0.8 Hz, 1H), 8.86 (dd, *J* = 2.1, 0.5 Hz, 1H), 8.03 (ddd, *J* = 8.3, 2.2, 0.8 Hz, 1H), 7.86 (dd, *J* = 8.3, 0.7 Hz, 1H). m.p. = 94.2-97.4 °C.

5-bromo-2-(dimethoxymethyl)pyridine: To a mixture of 5-bromopicolinaldehyde (2.13 g, 11.4 mmol) and *p*-toluenesulfonic acid monohydrate (390 mg, 2.26 mmol) in MeOH (40 ml) was added methyl orthoformate (6.1 ml, 55.7 mmol). The mixture was refluxed for 12 h and then evaporated under vacuum. The residue was dissolved in CH_2Cl_2, washed with saturated $NaHCO_3$ (aq) and dried over Na_2SO_4. The solvent was removed under vacuum to give a colourless oil (2.45 g, 93%). ^{1}H NMR (400 MHz, $CDCl_3$) δ 8.67 (dd, *J* = 2.3, 0.6 Hz, 1H), 7.87 (dd, *J* = 8.4, 2.3 Hz, 1H), 7.46 (d, *J* = 8.4 Hz, 1H), 5.35 (s, 1H), 3.39 (s, 6H).

2-(dimethoxymethyl)-5-(4,4,5,5-tetramethyl-1,3,2-dioxaborolan-2-yl)pyridine: A degassed solution of 5-bromo-2-(dimethoxymethyl)pyridine (2.45 g, 10.5 mmol), 4,4,4',4',5,5,5',5'-octamethyl-2,2'-bi(1,3,2-dioxaborolane) (2.67 g, 10.5 mmol), potassium acetate (2.6 g, 26.3 mmol) and Pd(dppf)Cl_2 (360 mg, 0.492 mmol) in anhydrous DMF (40 ml) was heated in Ar atmosphere at 50 °C for a day. The solvent was removed in vacuo and the residue was suspended in diethyl ether. The insoluble product was removed by filtration. The filtrate was concentrated in vacuo and then purified by column chromatography on silica gel (Hex/EA = 5:1) to give a light-yellow oil (2.49 g, 85%). ^{1}H NMR (400

MHz, $CDCl_3$) δ 8.68 (d, *J* = 1.8 Hz, 1H), 7.88 (dd, *J* = 8.4, 2.3 Hz, 1H), 7.47 (d, *J* = 8.4 Hz, 1H), 5.36 (s, 1H), 3.40 (s, 6H), 1.26 (s, 12H).

1,3,6,8-tetrakis(6-(dimethoxymethyl)pyridin-3-yl)pyrene **(TFPyriPy-Ac)**: A degassed mixture of 1,3,6,8-tetrabromopyrene (862 mg, 1.66 mmol), 2-(dimethoxymethyl)-5-(4,4,5,5-tetramethyl-1,3,2-dioxaborolan-2-yl)pyridine (2.45 g, 8.8 mmol), $Pd(PPh_3)_4$ (70 mg, 0.061 mmol), and K_2CO_3 (1.67 g, 12.1 mmol) in 1,4-dioxane (34 ml) was refluxed for 2 days. The mixture was cooled to room temperature and the solvent was removed in vacuo. The residue was suspended in $CHCl_3$ and filtered to remove insoluble products. The filtrate was dried in vacuo and then purified by column chromatography on silica gel (CH_2Cl_2, then CH_2Cl_2/MeOH = from 100:1 to 20:1) to give a yellow solid (781 mg, 58%). ^{1}H NMR (400 MHz, DMSO) δ 8.91 (d, *J* = 1.7 Hz, 4H), 8.25 – 8.18 (m, 8H), 7.73 (d, *J* = 8.0 Hz, 4H), 6.52 (s, 2H), 5.45 (s, 4H), 3.41 (s, 24H). ESI-HRMS Calcd. For $[C_{48}H_{46}N_4O_8+H]$ 807.3388, found 807.3386. m.p. = 252 °C (decomposition).

5,5′,5′′,5′′′-(pyrene-1,3,6,8-tetrayl)tetrapicolinaldehyde **(TFPyriPy)**: **TFPyriPy-Ac** (80.7 mg, 0.1 mmol) was suspended in a mixture of THF (25 ml) and HCl (2 M aq, 20 ml) under Ar atmosphere. The reaction was stirred at room temperature for 12 h. The pH of the mixture was adjusted to ~8 and THF was removed in vacuo. The insoluble solid was filtered, washed by water and MeOH, and dried to give a brown colour solid (56 mg, 90%). ^{1}H NMR (400 MHz, $CDCl_3$) δ 10.24 (s, 4H), 9.11 (s, 4H), 8.20 (d, *J* = 10.5 Hz, 10H), 8.13 – 7.97 (m, 4H). m.p. > 300 °C (decomposition).

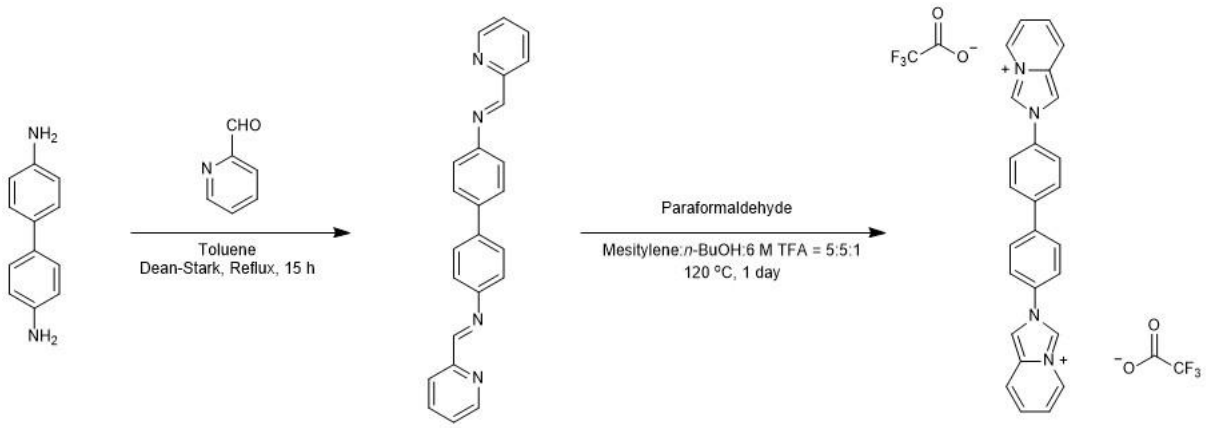

Supplementary Fig. 2 | Synthesis of the model compound of imidazopyridinium COFs.

COF model compound (IP-model-1): A mixture of benzidine (184 mg, 1 mmol) and picolinaldehyde (0.95 ml, 10 mmol) was refluxed in toluene (10 ml) with a Dean-Stark trap for 15 h. The solvent of the mixture was removed in vacuo and the solid residue was washed with methanol and dried to afford the imine compound in beige colour without further purification. To a 10 ml Schlenk tube (15 mm × 80 mm) was added with the imine compound (7.2 mg, 0.02 mmol) and paraformaldehyde (7.2 mg, 0.24 mmol), mesitylene (0.5 ml), and *n*-butanol (0.5 ml). The mixture was sonicated for 2 mins, added with 6 M trifluoroacetic acid (100 μl), flash frozen at 77 K, and degassed under freeze-pump-thaw for three cycles. The tube was then sealed and heated at 120 °C in an oven for one day. The mixture was cooled to room temperature and a brown colour needle-like crystal was precipitated, which was collected for X-ray analysis (12.3 mg, > 99%). ^{1}H NMR (400 MHz, DMSO) δ 10.42 (s, 2H), 8.84 (s, 2H), 8.62 (d, *J* = 6.2 Hz, 2H), 8.22 – 8.16 (m, 4H), 8.10 – 8.05 (m, 4H), 7.96 (d, *J* = 9.4 Hz, 2H), 7.40 – 7.34 (m, 2H), 7.32 – 7.27 (m, 2H). ^{13}C NMR (101 MHz, DMSO) δ 157.63, 140.09, 134.92, 129.82, 128.73, 125.88, 125.31, 124.25, 123.37, 118.80, 118.33, 118.30, 112.13. ESI-HRMS Calcd. For $[C_{26}H_{20}N_4^{2+}]$ 194.0838, found 194.0845. m.p. = 211.2-212.5 °C.

Synthetic Procedure of the COFs

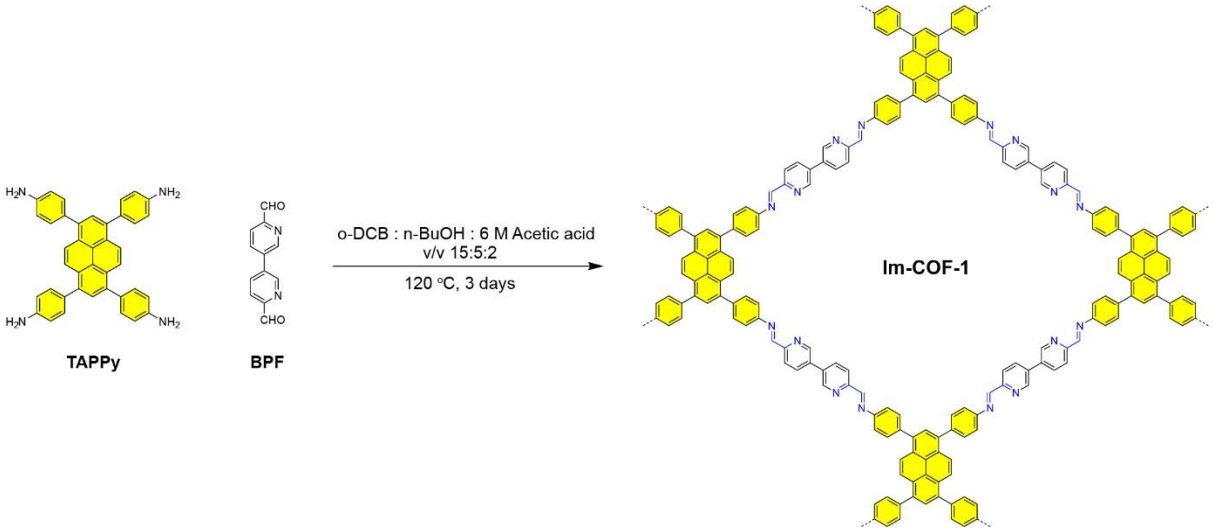

Supplementary Fig. 3 | Synthesis of Im-COF-1.

Im-COF-1: To a 10 ml Schlenk tube (15 mm × 80 mm) was added with **TAPPy** (11.3 mg, 0.02 mmol), **BPF** (8.5 mg, 0.04 mmol), *o*-DCB (0.75 ml) and *n*-BuOH (0.25 ml). The mixture was sonicated for 2 mins, added with 6 M acetic acid (100 μl), flash frozen at 77 K, and degassed under freeze-pump-thaw for three cycles. The tube was then sealed and heated at 120 °C in an oven for three days. The solid obtained was exchanged with THF (5 ml) for 5 times and dried under vacuum to afford an orange solid (17 mg, 92%). Anal. Calcd. for $(C_{64}H_{42}N_8 \cdot 4.1\ H_2O)_n$: C 77.11; H 5.08; N 11.24; found: C 76.49; H 4.40; N 11.18.

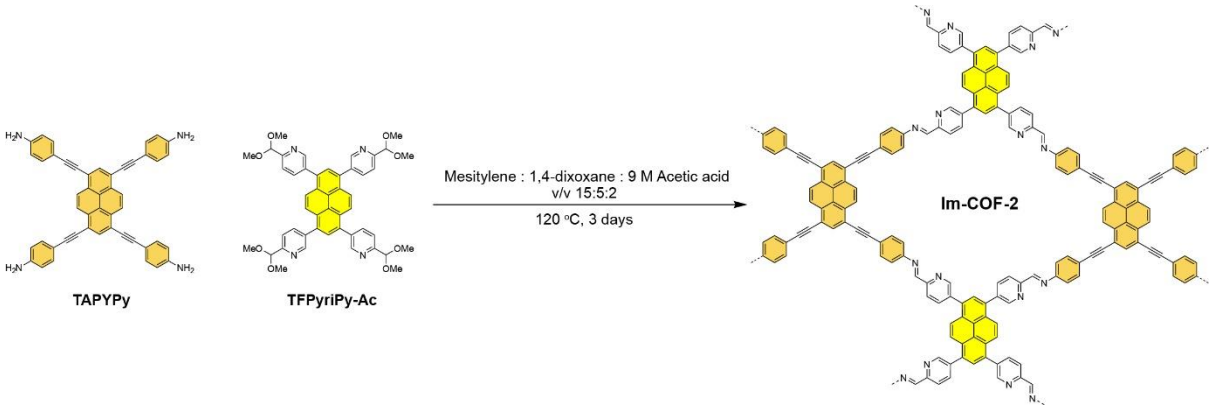

Supplementary Fig. 4 | Synthesis of Im-COF-2.

Im-COF-2: To a 10 ml Schlenk tube (15 mm × 80 mm) was added with **TAPYPy** (13.3 mg, 0.02 mmol), **TFPyriPy-Ac** (16.1 mg, 0.02 mmol), mesitylene (0.75 ml) and 1,4-dioxane (0.25 ml). The mixture was sonicated for 2 mins, added with 9 M acetic acid (100 μl), flash frozen at 77 K, and degassed under freeze-pump-thaw for three cycles. The tube was then sealed and heated at 120 °C in an oven for three days. The solid obtained was exchanged with THF (5 ml) for 5 times and dried under vacuum to afford a red solid (20.9 mg, 87%). Anal. Calcd. for $(C_{88}H_{44}N_8 \cdot 11.65\ H_2O)_n$: C 74.26; H 4.77; N 7.87; found: C 73.32; H 3.82; N 7.36.

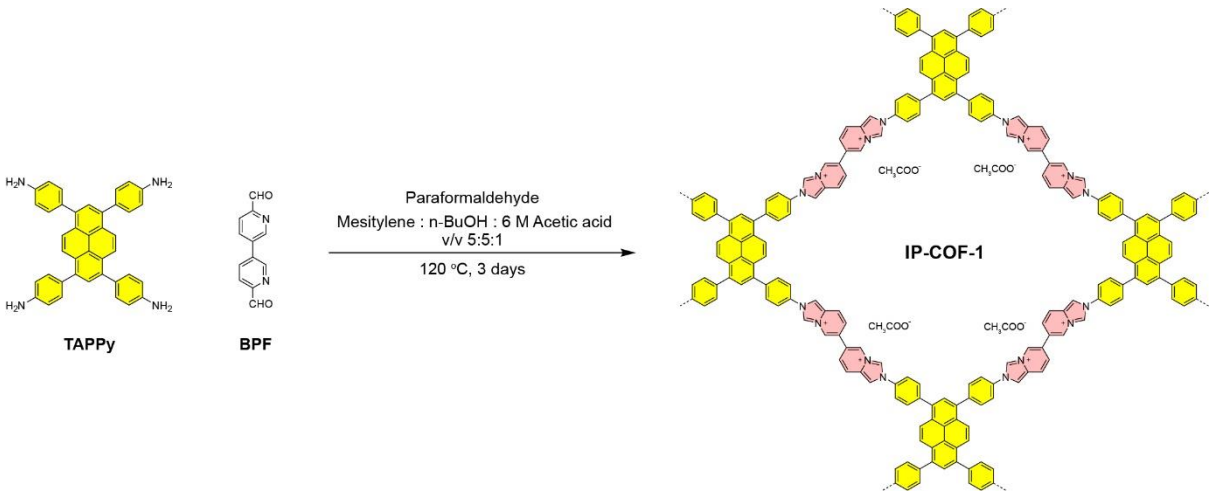

Supplementary Fig. 5 | One-pot synthesis of IP-COF-1.

IP-COF-1 (one-pot): A mixture of **TAPPy** (11.3 mg, 0.02 mmol) and paraformaldehyde (7.2 mg, 0.24 mmol) in *n*-BuOH (0.5 ml) was stirred at room temperature for 30 min. Then the mixture was added to a 10 ml Schlenk tube (15 mm × 80 mm) charged with **BPF** (8.5 mg, 0.04 mmol) in mesitylene (0.5 ml). The mixture was sonicated for 2 min and added with 6 M acetic acid (100 μl). The suspension was flash frozen at 77 K, and degassed under freeze-pump-thaw for three cycles. The tube was then sealed and heated at 120 °C in an oven for three days. The solid obtained was exchanged with THF (5 ml) for three times, water (5 ml) for two times and THF (5 ml) for another two times, and dried under vacuum to afford an orange solid (19.9 mg, 82%). Anal. Calcd. for $(C_{76}H_{58}N_8O_8 \cdot 0.4\ H_2O)_n$: C 74.91; H 4.86; N 9.2; found: C 73.97; H 4.33; N 10.15.

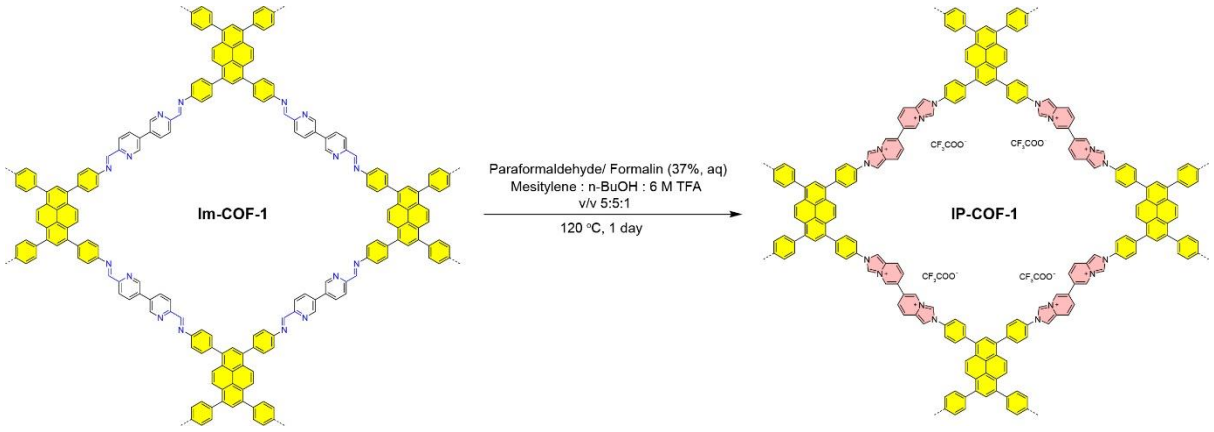

Supplementary Fig. 6 | Synthesis of IP-COF-1 from Im-COF-1.

IP-COF-1 (paraformaldehyde): To a 10 ml Schlenk tube (15 mm × 80 mm) was added with Im-COF-1 (18.4 mg, 0.02 mmol), paraformaldehyde (7.2 mg, 0.24 mmol), mesitylene (0.5 ml) and *n*-BuOH (0.5 ml). The mixture was briefly sonicated for ~10 s. The mixture turned black immediately upon added with 6 M trifluoroacetic acid (100 μl). The suspension was flash frozen at 77 K, and degassed under freeze-pump-thaw for three cycles. The tube was then sealed and heated at 120 °C in an oven for one day. The solid obtained was exchanged with THF (5 ml) for three times, water (5 ml) for two times and THF (5 ml) for another two times, and dried under vacuum to afford an orange solid (17.3 mg, 61%). Anal. Calcd. for $(C_{76}H_{46}N_8O_8F_{12} \cdot 2.25\ C_4H_8O \cdot 3.95\ H_2O)_n$: C 61.48; H 4.36; N 6.75; found: C 61.49; H 4.38; N 6.76.

IP-COF-1 (formalin solution): To a 10 ml Schlenk tube (15 mm × 80 mm) was added with Im-COF-1 (18.4 mg, 0.02 mmol), formalin solution (20 μl, 37%, aq), mesitylene (0.5 ml) and *n*-BuOH (0.5 ml). The mixture was briefly sonicated for ~10 s. The mixture turned black immediately upon added with 6 M trifluoroacetic acid (100 μl). The suspension was flash frozen at 77 K, and degassed under freeze-pump-thaw for three cycles. The tube was then sealed and heated at 120 °C in an oven for one day. The solid obtained was exchanged with THF (5 ml) for three times, water (5 ml) for two times and THF (5 ml) for another two times, and dried under vacuum to afford an orange solid (18.4 mg, 65%). Anal. Calcd. for $(C_{76}H_{46}N_8O_8F_{12} \cdot 1.95\ C_4H_8O \cdot 4.4\ H_2O)_n$: C 61.11; H 4.31; N 6.8; found: C 61.11; H 4.28; N 6.78.

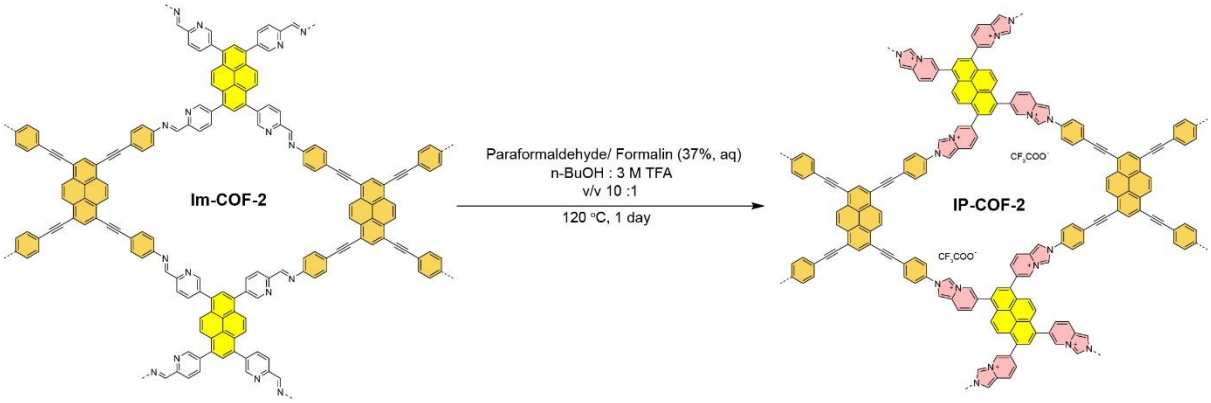

Supplementary Fig. 7 | Synthesis of IP-COF-2 from Im-COF-2.

IP-COF-2: To a 10 ml Schlenk tube (15 mm × 80 mm) was added with Im-COF-2 (24 mg, 0.02 mmol), paraformaldehyde (7.2 mg, 0.24 mmol) or formalin (37%, aq), and *n*-BuOH (1 ml). The mixture was briefly sonicated for ~10 s. The mixture turned black immediately upon added with 3 M trifluoroacetic acid (100 μl). The suspension was flash frozen at 77 K, and degassed under freeze-pump-thaw for three cycles. The tube was then sealed and heated at 120 °C in an oven for one day. The solid obtained was exchanged with THF (5 ml) for three times, water (5 ml) for two times and THF (5 ml) for another two times, and dried under vacuum to afford a red solid (23.5 mg, 68%). Anal. Calcd. for $(C_{100}H_{48}N_8O_8F_{12} \cdot 2.7\ C_4H_8O)_n$: C 69.6; H 3.67; N 5.86; found: C 69.98; H 4.42; N 6.62.

Method for Li-S battery assembly and related electrochemical test

Preparation of IP-COF-1/S, Im-COF-1/S and KB/S composites

For low-loading sulfur cathode, IP-COF-1, Ketjenblack (KB, EC 600JD) and sulfur powder were grinded at a ratio of 5:25:70 for 30 minutes to form a uniform mixture. Then the mixture was heated at 155 °C for 12 h to obtain the IP-COF-1/S composite. The same method was employed in preparing Im-COF-1/S and KB/S composites by replacing IP-COF-1 with Im-COF-1 and KB, respectively. For high-loading cathode, the IP-COF-1/S composite consists of 5% IP-COF-1, 15% conductive agent (KB) and 80% sulfur. The percentages of sulfur in different IP-COF-1/S composites were verified by the TGA test.

Electrochemical measurements

Working electrodes of lithium-sulfur batteries contain 80 wt% active sample (IP-COF-1/S, Im-COF-1/S or KB/S composites), 8 wt% binder (PVDF for low-loading cathode and LA133 for high-loading cathode), and 12 wt% conductive carbon (MWCNTs/Super P = 1:1). The average sulfur loading for low-loading cathode was 0.8~1 mg cm^{-2}, while the loading for high-loading cathode was ~9 mg cm^{-2}. The specific capacity of each cell is calculated by the mass of sulfur. The electrolyte in batteries containing 1 M lithium bis(trifluoromethanesulfonyl)imide (LiTFSI) in 1,2-dimethoxyethane (DME)/1,3-dioxolane (DOL) (v/v, 1:1) with additional 2.0 wt% $LiNO_3$. Celgard 2500 was used as the separator. The electrolyte/sulfur (E/S) ratio of the cells was 15 $\mu L_E\ mg_S^{-1}$ for low-sulfur-loading cathode and 6 $\mu L_E\ mg_S^{-1}$ for high-sulfur-loading cathode. The cells were galvanostatically cycled between 1.8–2.7 V on the Land 8-channel battery cycler under different C-rates (1 C = 1675 mA g^{-1}). CV and EIS were conducted on an Autolab electrochemical workstation. CV measurement was performed at a scan rate of 0.1~0.5 mV s^{-1} between 1.8 and 2.7 V. EIS was performed using the potentiostatic mode at the open-circuit potential. A sinusoidal voltage with an amplitude of 10 mV and a frequency range from 10^{-1} Hz to 10^{6} Hz were applied.

Preparation of Li_2S_8 solution

The whole preparation was carried out in an argon gas-filled glove box. The Li_2S_8/Li_2S_6 solution was synthesized *via* dissolving lithium sulfide (Li_2S) and sulfur with a stoichiometric ratio (1:7/1:5) in the pre-mixed solution (1.0 M LiTFSI in DOL/DME [v/v = 1:1]) and then magnetically stirring over night at 60 °C.

Evaluation of polysulfides kinetics

The carbon paper (CP) electrodes adopted for the symmetric cells or potentiostatic intermittent titration technique (PITT) contain 40 wt% active sample (IP-COF-1, Im-COF-1 or KB), 10 wt% poly(vinylidene difluoride) (PVDF), and 50 wt% Super-P. The cathodes were made by drop-casting method on carbon paper substrates (14 mm in diameter), with an average active material loading of ~0.6 mg cm^{-2}. For Li_2S_6 symmetric cells, 40 μL of Li_2S_6 (0.5 M) and LiTFSI (1 M) in DOL/DME (v/v = 1:1) was used as the electrolyte. CV curves of the symmetric cells were recorded at a scan rate of 10 mV s^{-1} between −0.8 and 0.8 V.

For PITT test, Li||CP/polysulfide cells were assembled using as-formed CP electrodes as cathode, Li foil (0.5 mm in thickness and 16 mm in diameter) as the anode, and PP as the separator. 20 μl of Li_2S_8 (0.5 M) and LiTFSI (0.5 M) in DOL/DME (v/v = 1:1) was used as the catholyte. 10 μl of LiTFSI (0.5 M) in DOL/DME (v/v = 1:1) was used as the anolyte for lithium surface wetting. The total sulfur content in each cell was 2.56 mg. PITT was conducted on the Autolab electrochemical workstation. The cells were first rest at the open-circuit voltage for 2.0 h, and the duration for a given step was 2.0 or 4.0 h to ensure the full conversion of polysulfides.

Screening the Synthetic Conditions of COFs

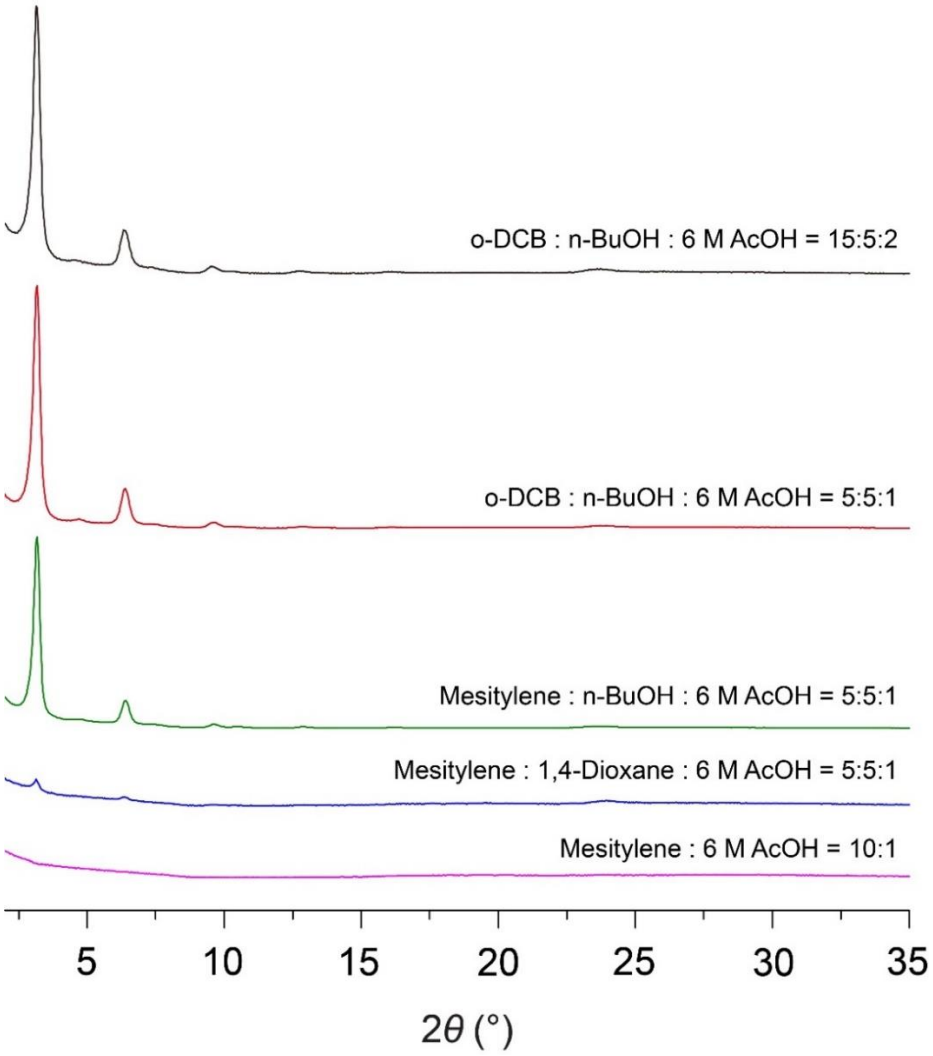

Supplementary Fig. 8 | PXRD patterns of Im-COF-1 synthesized *via* various conditions.

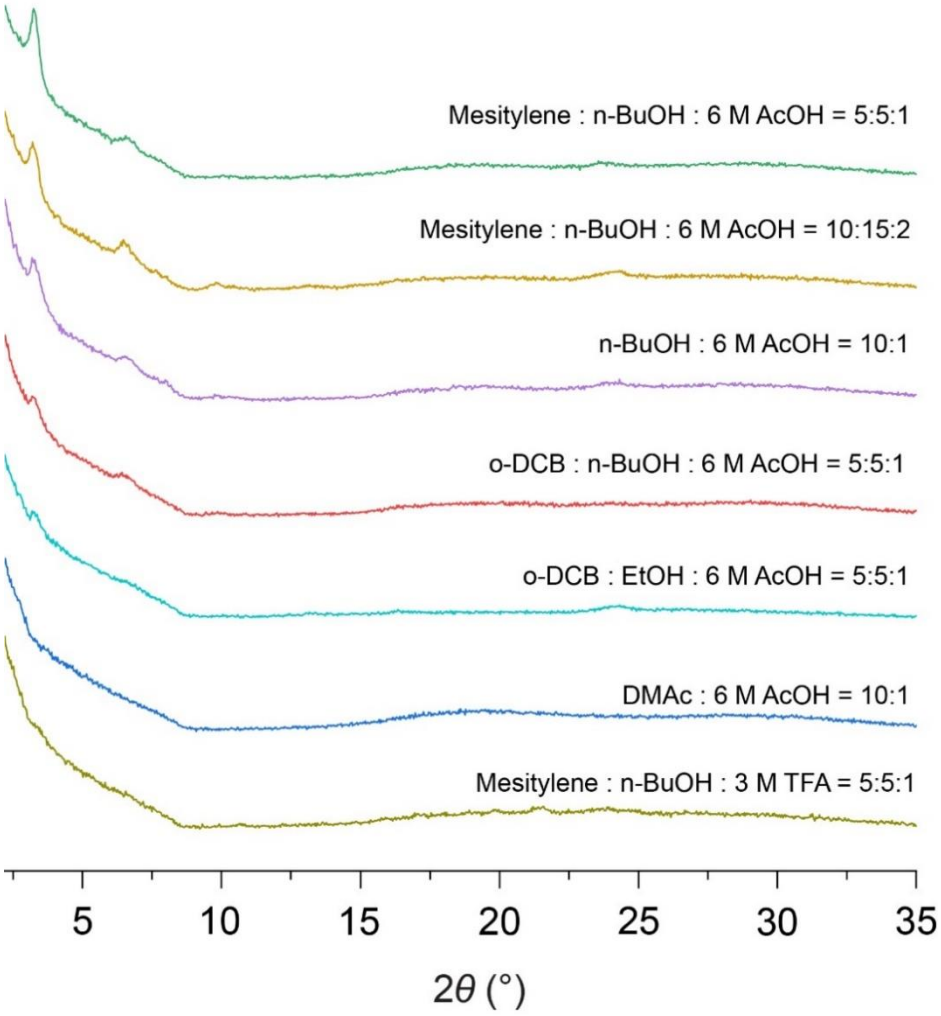

Supplementary Fig. 9 | PXRD patterns of IP-COF-1 synthesized *via* various conditions using the one-pot method.

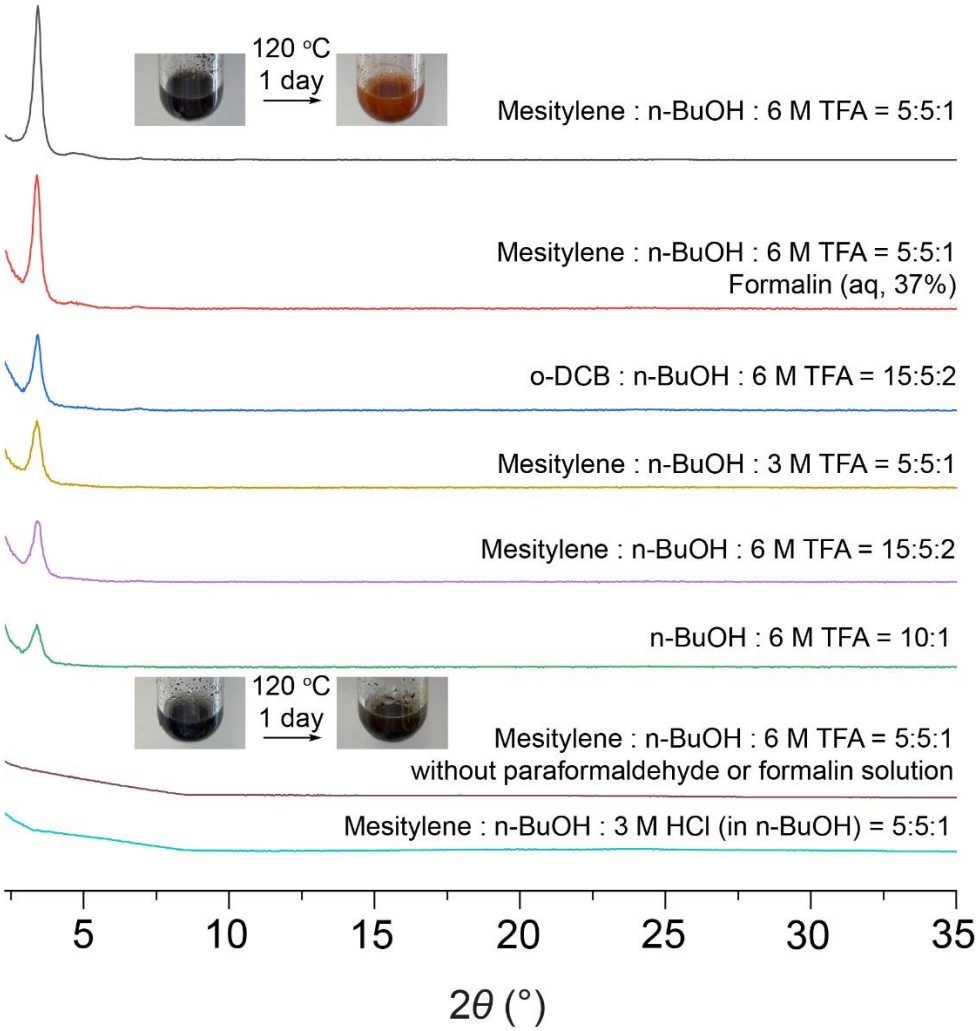

Supplementary Fig. 10 | PXRD patterns of IP-COF-1 synthesized *via* various conditions using the two-step method. Paraformaldehyde was used as the precursor unless specified.

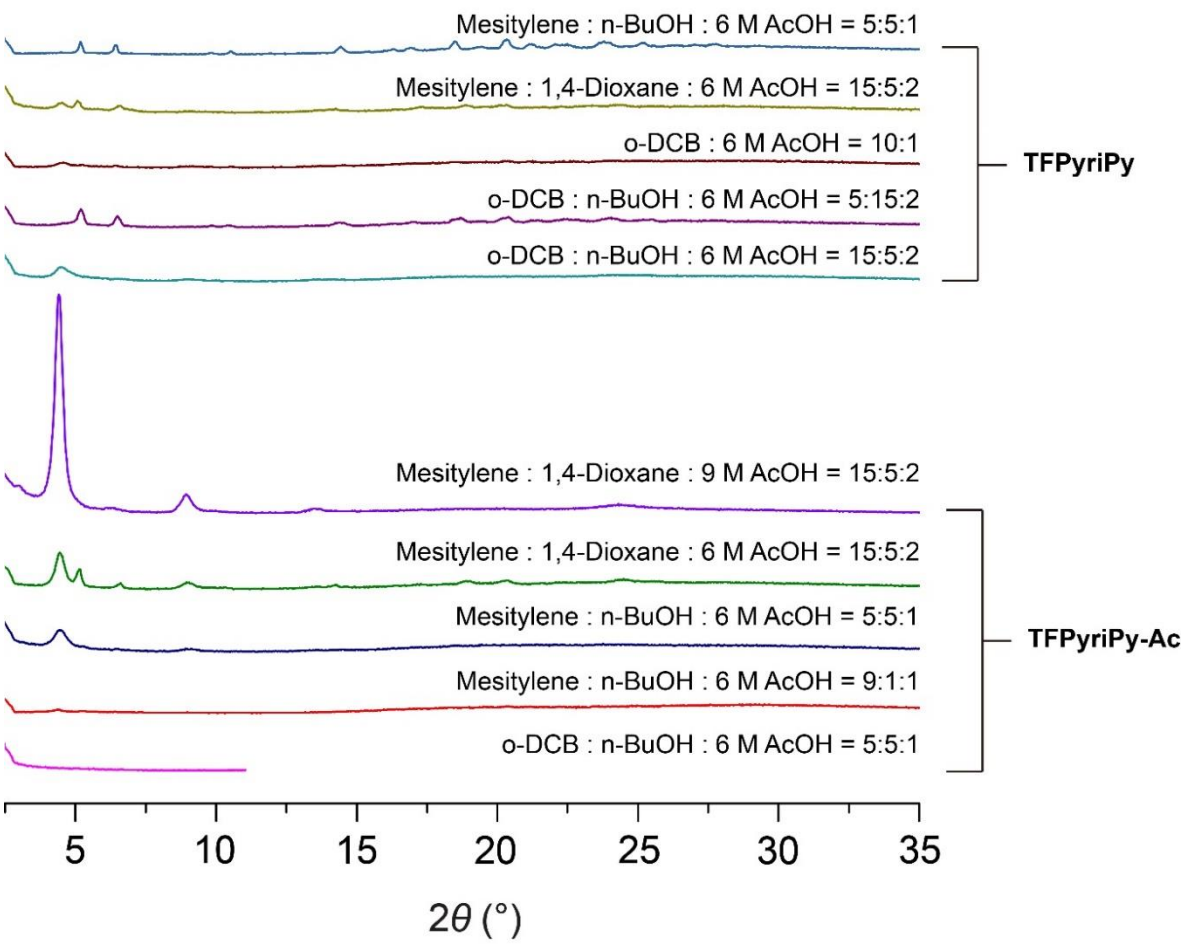

Supplementary Fig. 11 | PXRD patterns of Im-COF-2 synthesized *via* various conditions.

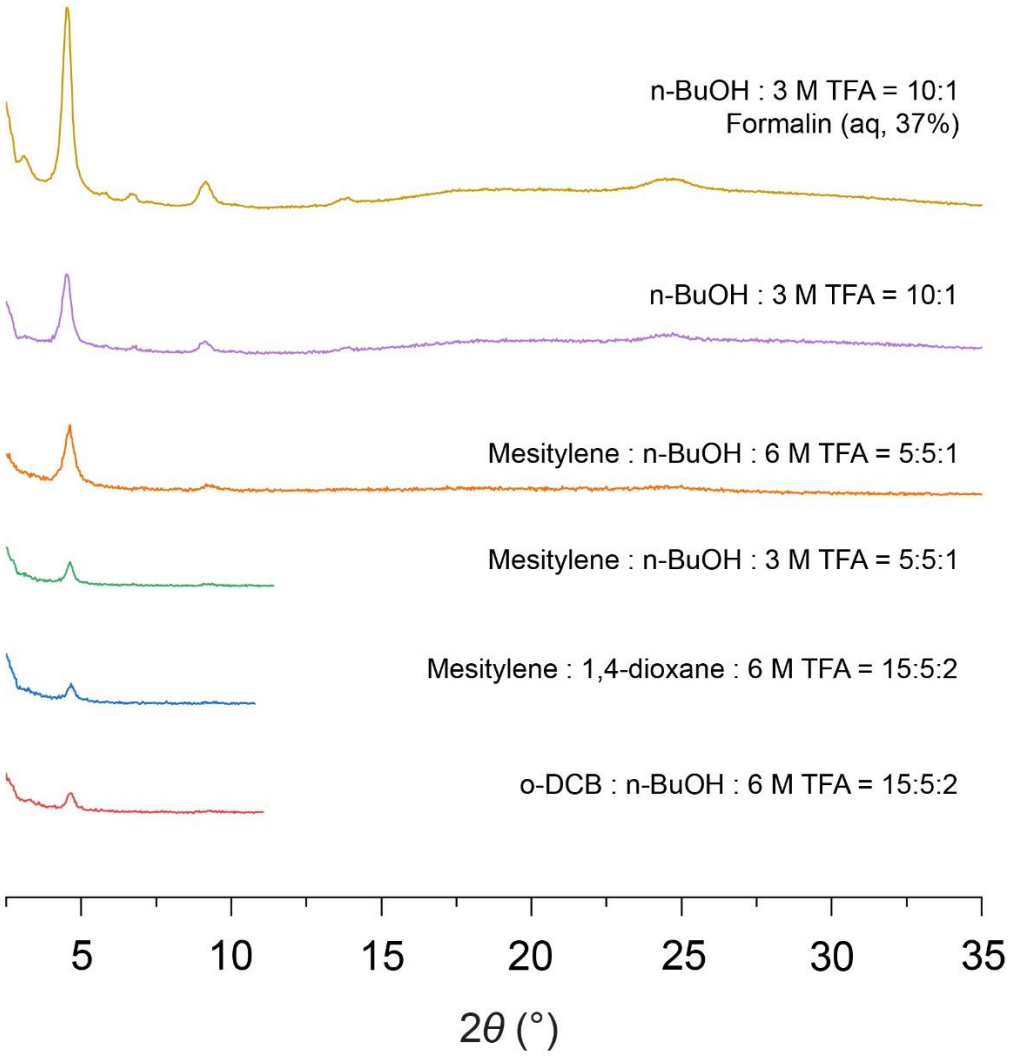

Supplementary Fig. 12 | PXRD patterns of IP-COF-2 synthesized *via* various conditions using the two-step method. Paraformaldehyde was used as the precursor unless specified.

FT-IR

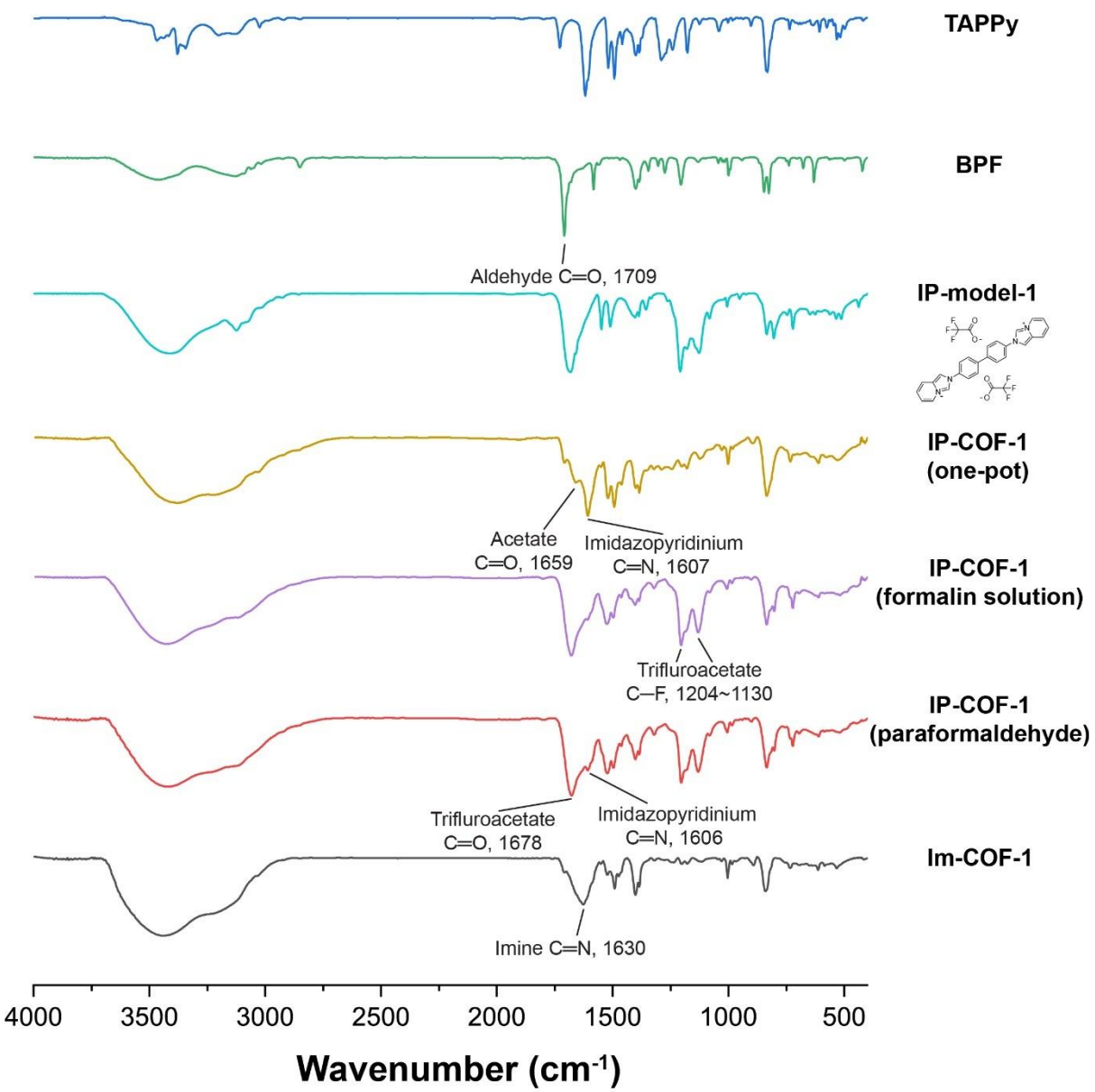

Supplementary Fig. 13 | FT-IR of Im-COF-1, IP-COF-1, model compound and their building units.

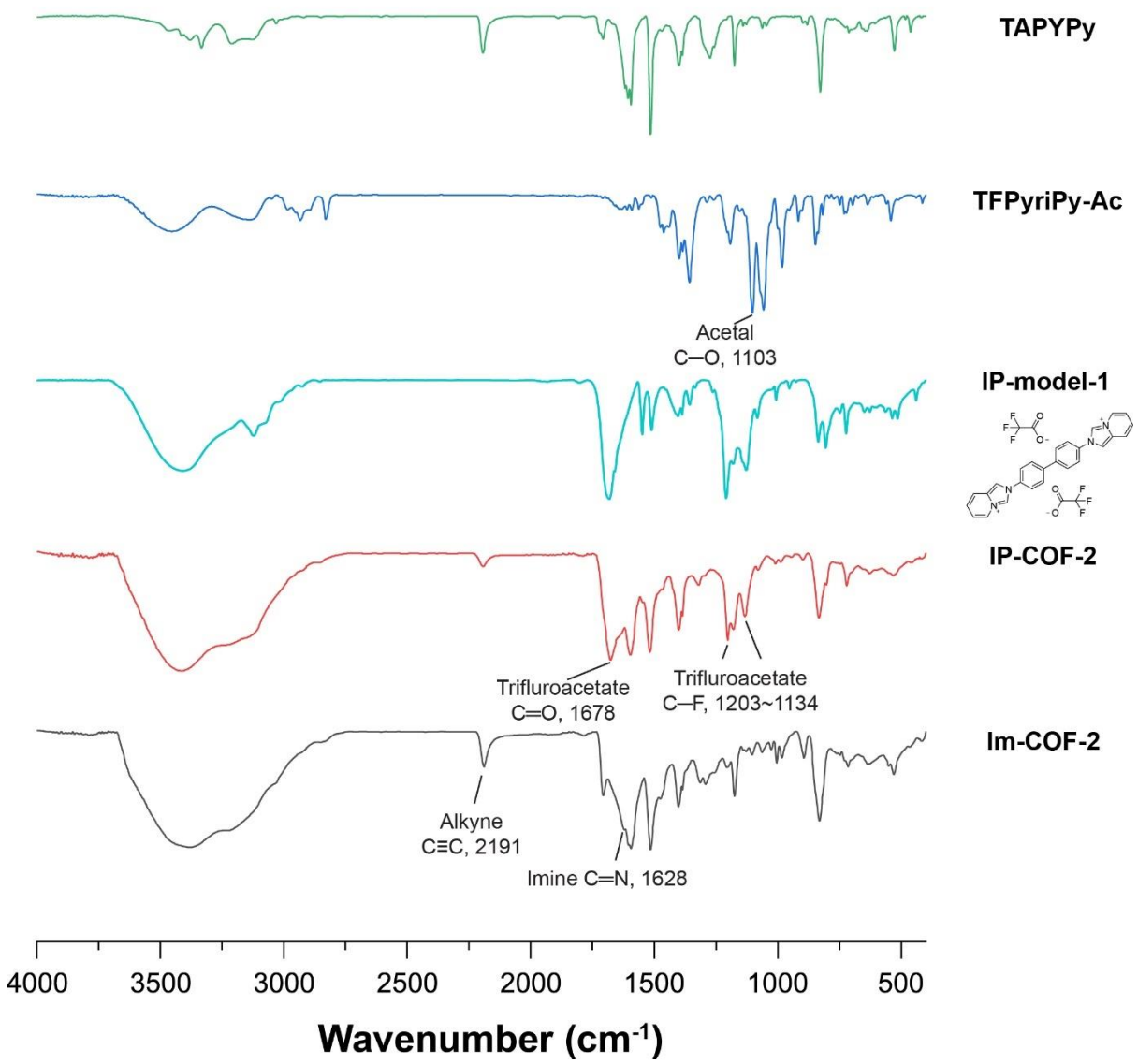

Supplementary Fig. 14 | FT-IR of Im-COF-2, IP-COF-2, model compound and their building units.

Solid-state NMR

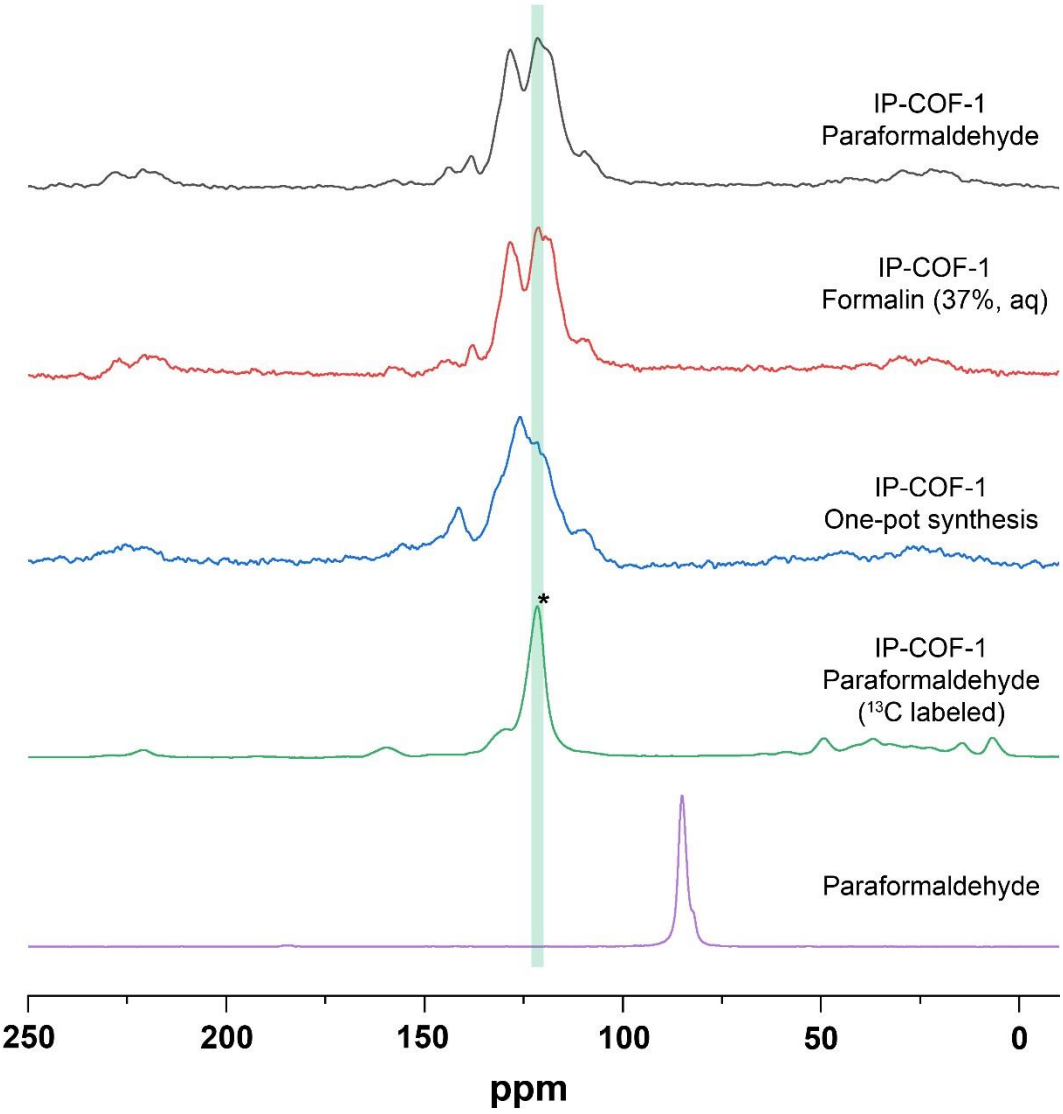

Supplementary Fig. 15 | Solid-state CP/MAS ^{13}C NMR spectra of Im-COF-1, IP-COF-1, ^{13}C-labeled IP-COF-1 and paraformaldehyde.

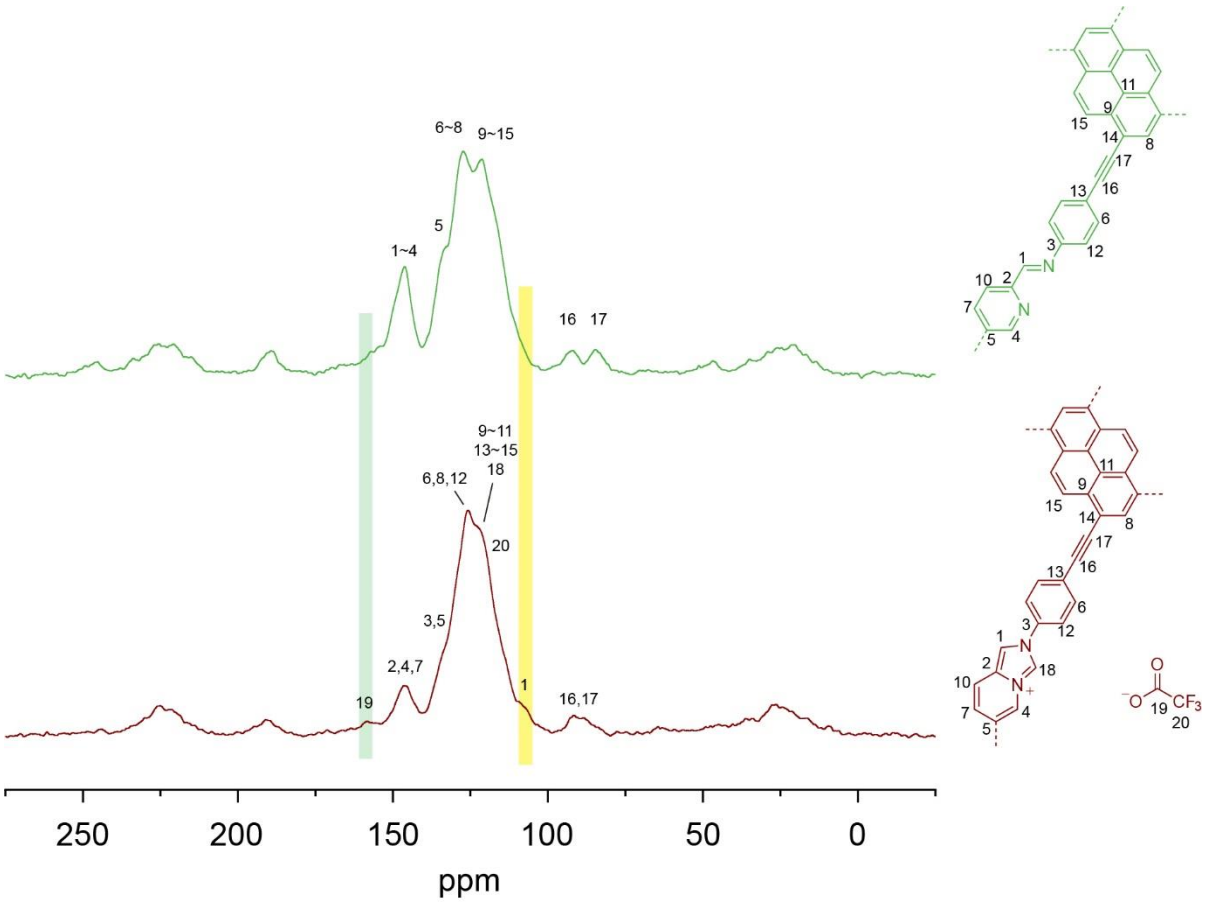

Supplementary Fig. 16 | Solid-state CP/MAS ^{13}C NMR spectra of Im-COF-2, and IP-COF-2.

Proposed mechanisms for imidazopyridinium bond formation in COFs

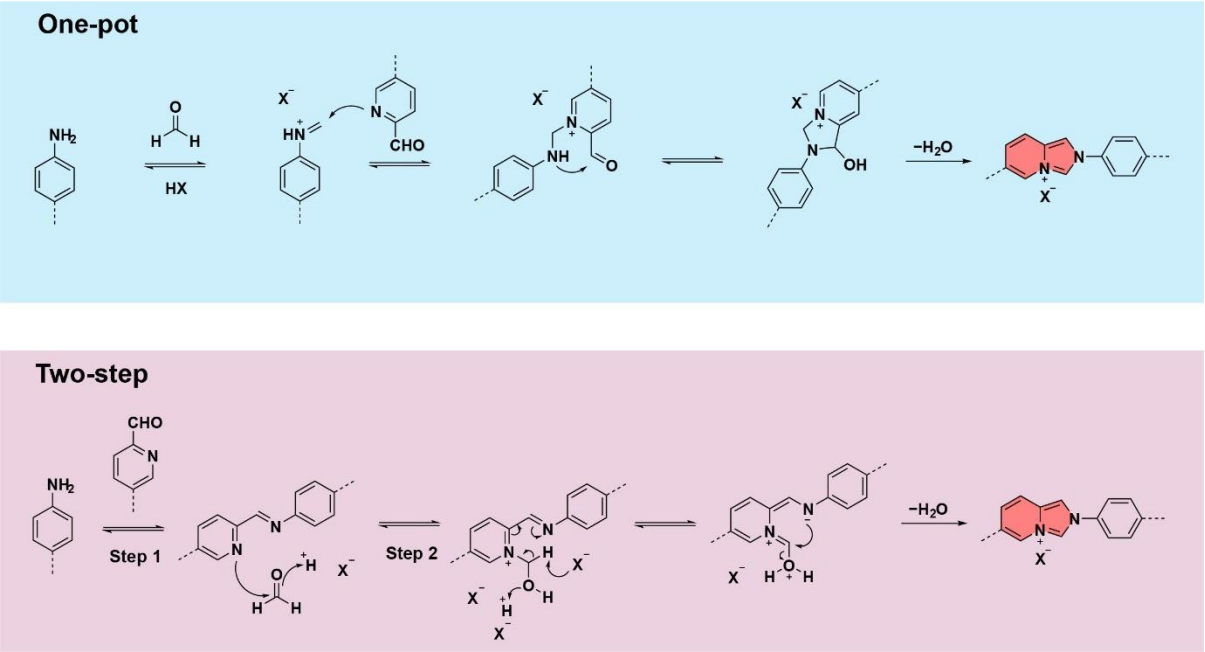

Supplementary Fig. 17 | Proposed mechanisms for the imidazopyridinium bond formation via the one-pot and the two-step pathway, respectively.

Confirming the crystal structures of COFs

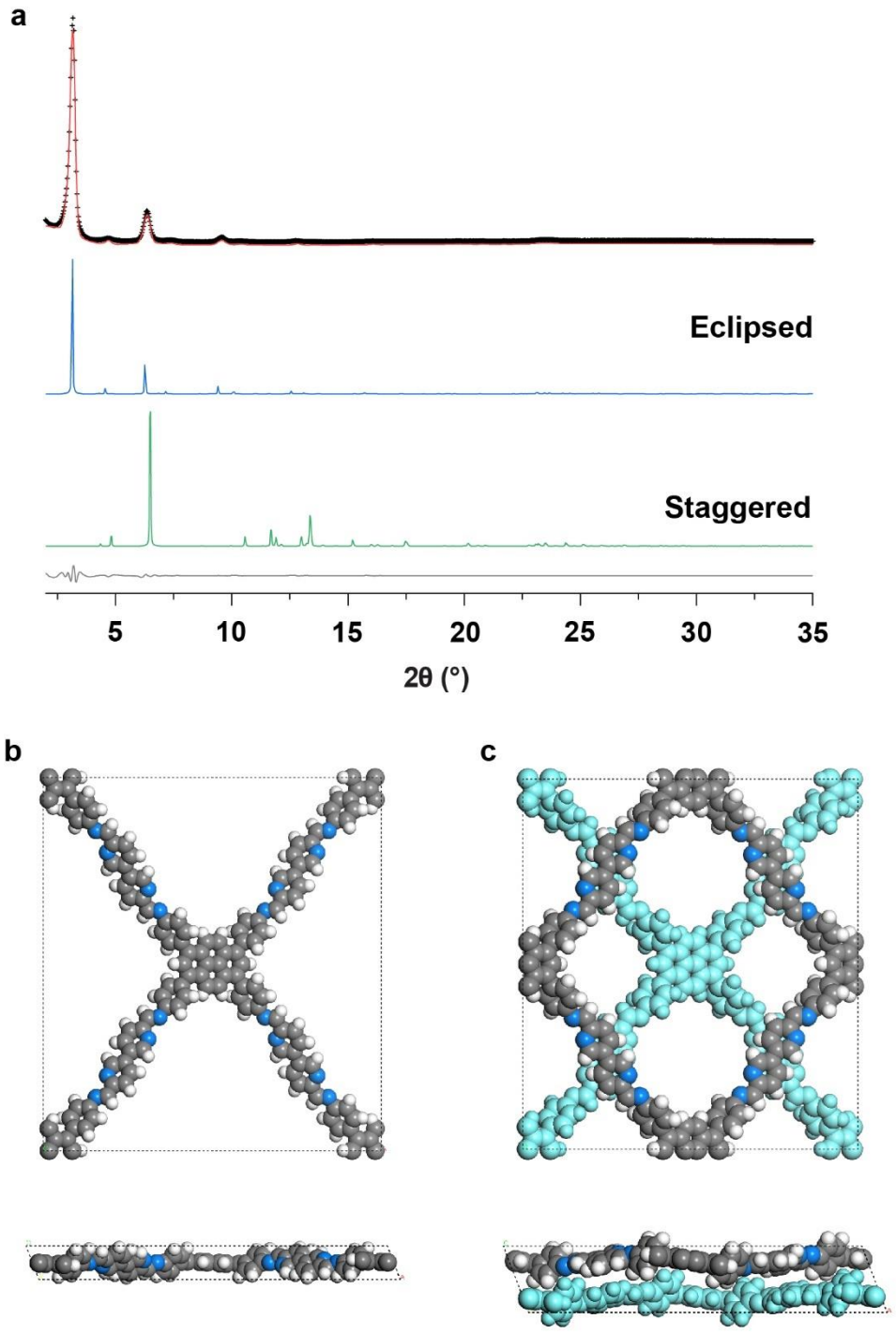

Supplementary Fig. 18 | Structural determination of Im-COF-1. a, PXRD patterns of Im-COF-1 (experimental: black; Pawley refined: red; Difference: grey; simulated eclipsed stacking: blue; simulated staggered stacking: green). Pawley-refined structures of **b**, eclipsed stacking and **c**, staggered stacking.

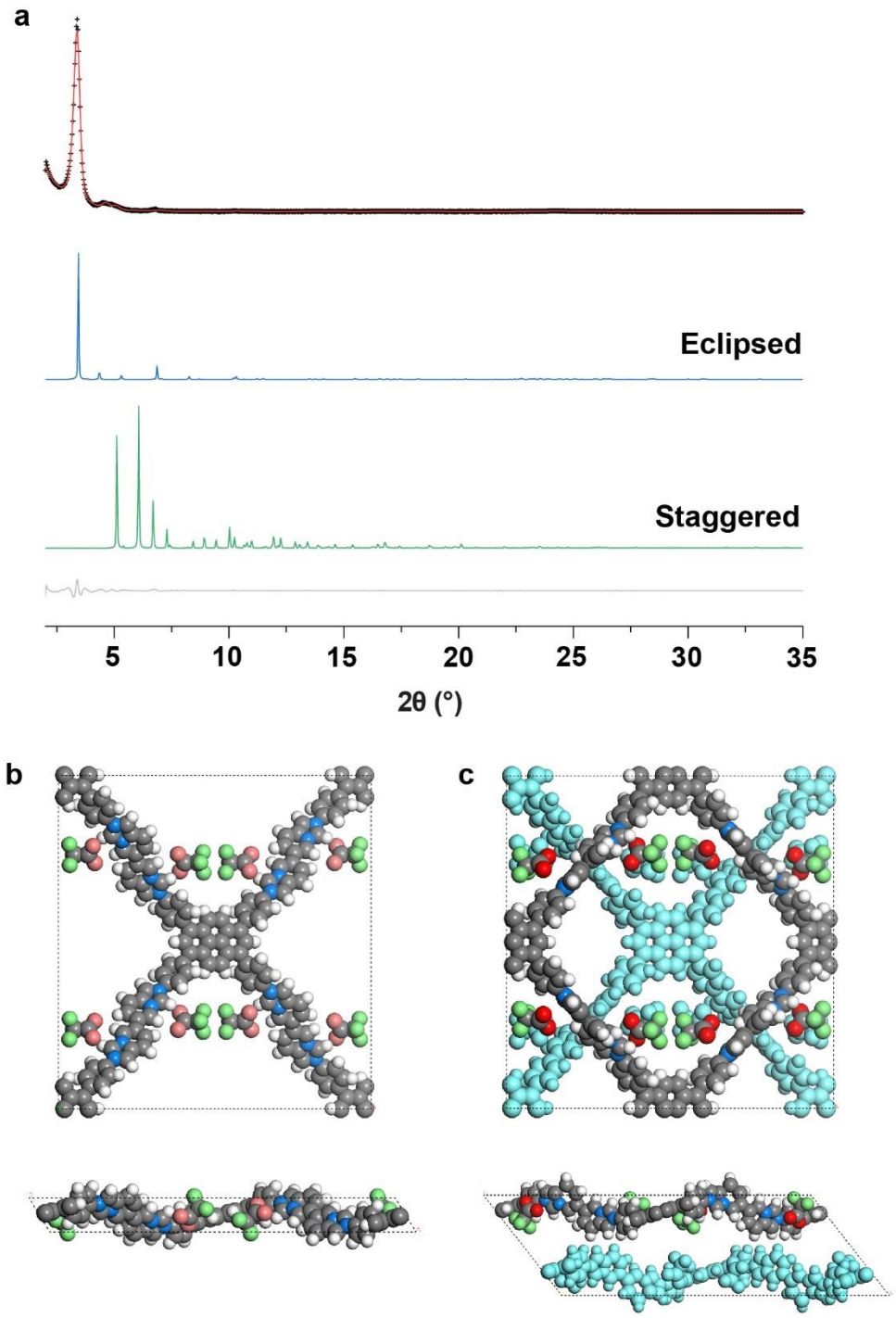

Supplementary Fig. 19 | Structural determination of IP-COF-1. a, PXRD patterns of IP-COF-1 (experimental: black; Pawley refined: red; Difference: grey; simulated eclipsed stacking: blue; simulated staggered stacking: green). Pawley-refined structures of **b**, eclipsed stacking and **c**, staggered stacking.

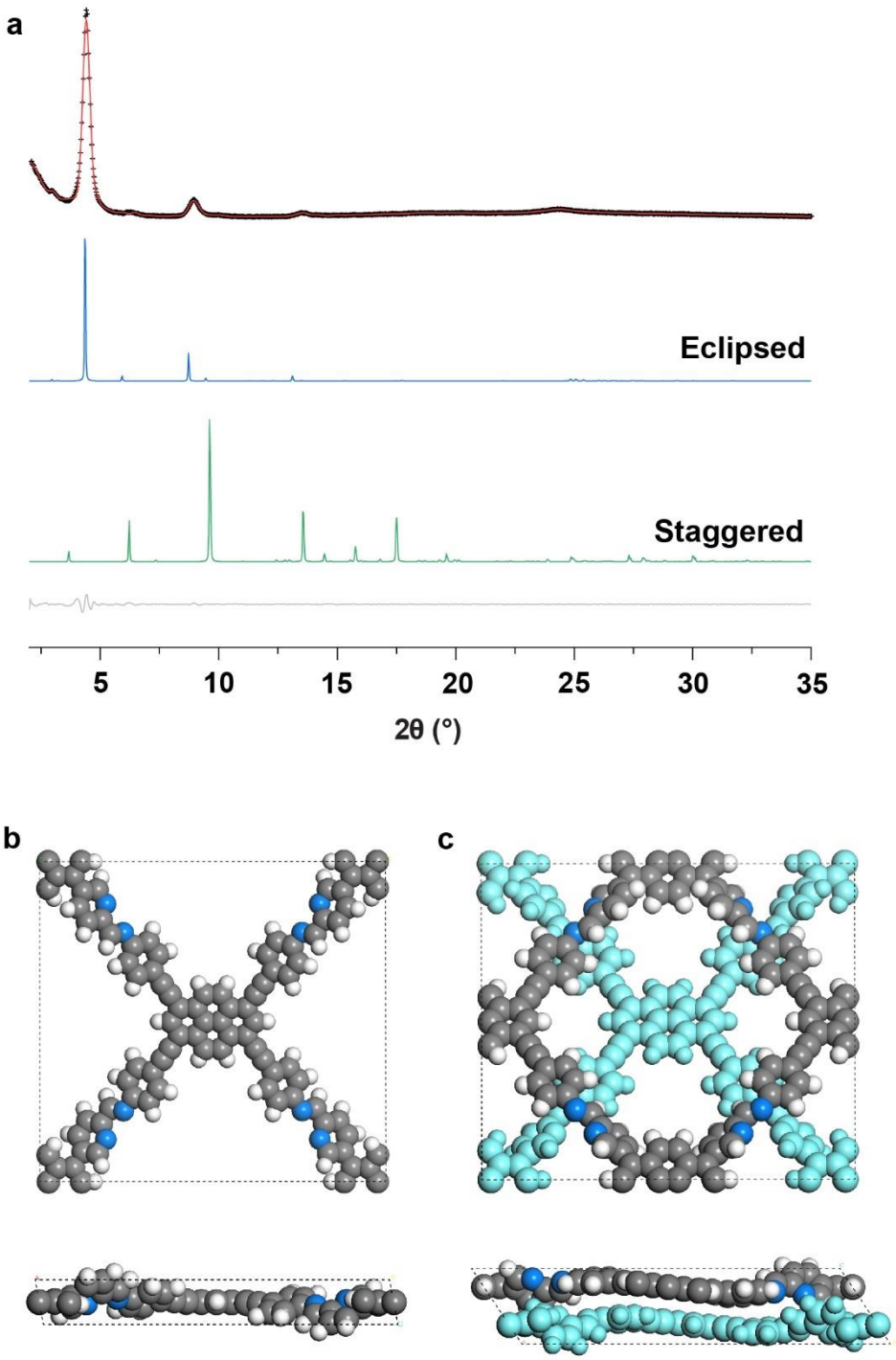

Supplementary Fig. 20 | Structural determination of Im-COF-2. a, PXRD patterns of Im-COF-2 (experimental: black; Pawley refined: red; Difference: grey; simulated eclipsed stacking: blue; simulated staggered stacking: green). Pawley-refined structures of **b**, eclipsed stacking and **c**, staggered stacking.

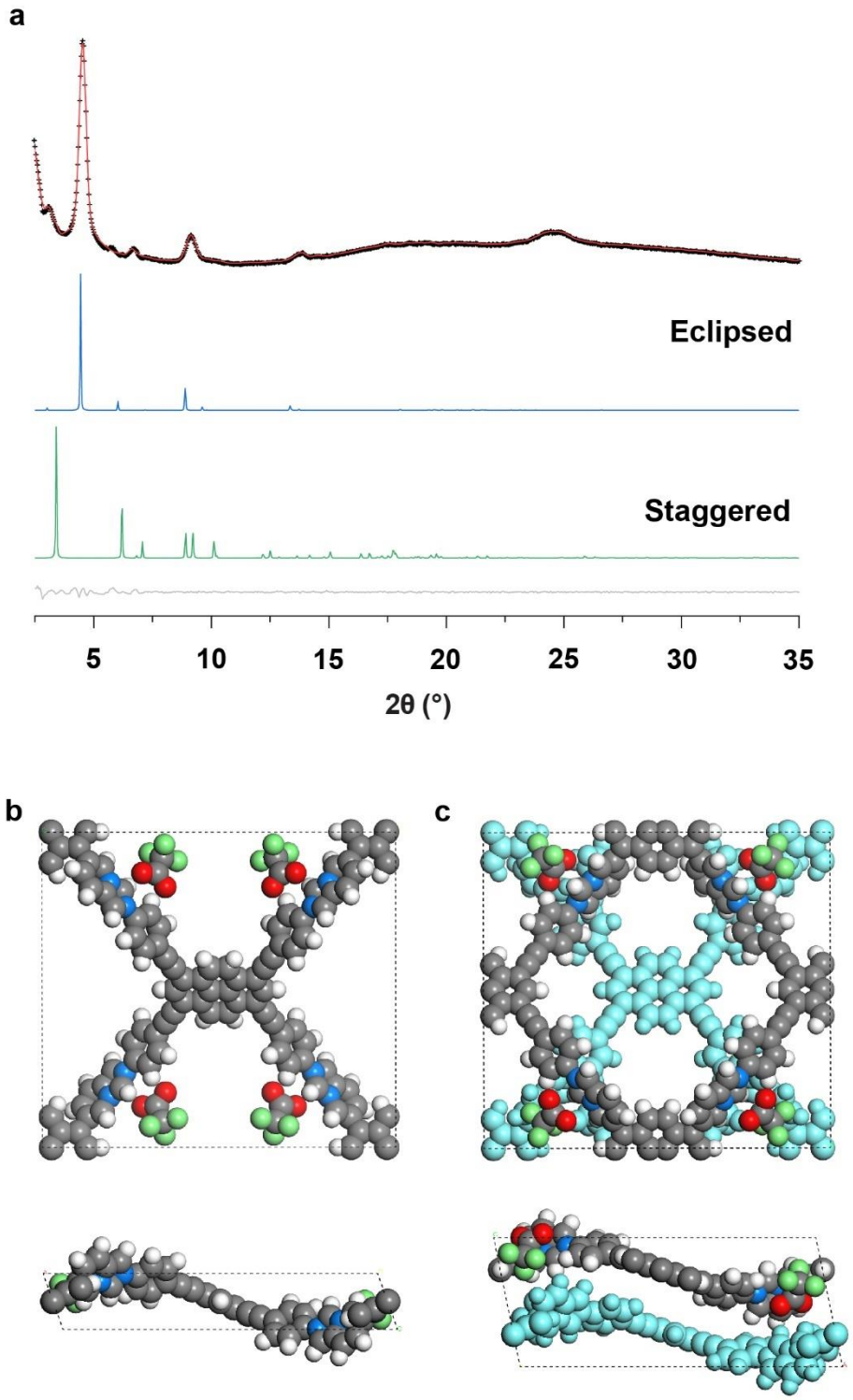

Supplementary Fig. 21 | Structural determination of IP-COF-2. a, PXRD patterns of IP-COF-2 (experimental: black; Pawley refined: red; Difference: grey; simulated eclipsed stacking: blue; simulated staggered stacking: green). Pawley-refined structures of **b**, eclipsed stacking and **c**, staggered stacking.

Nitrogen sorption experiments

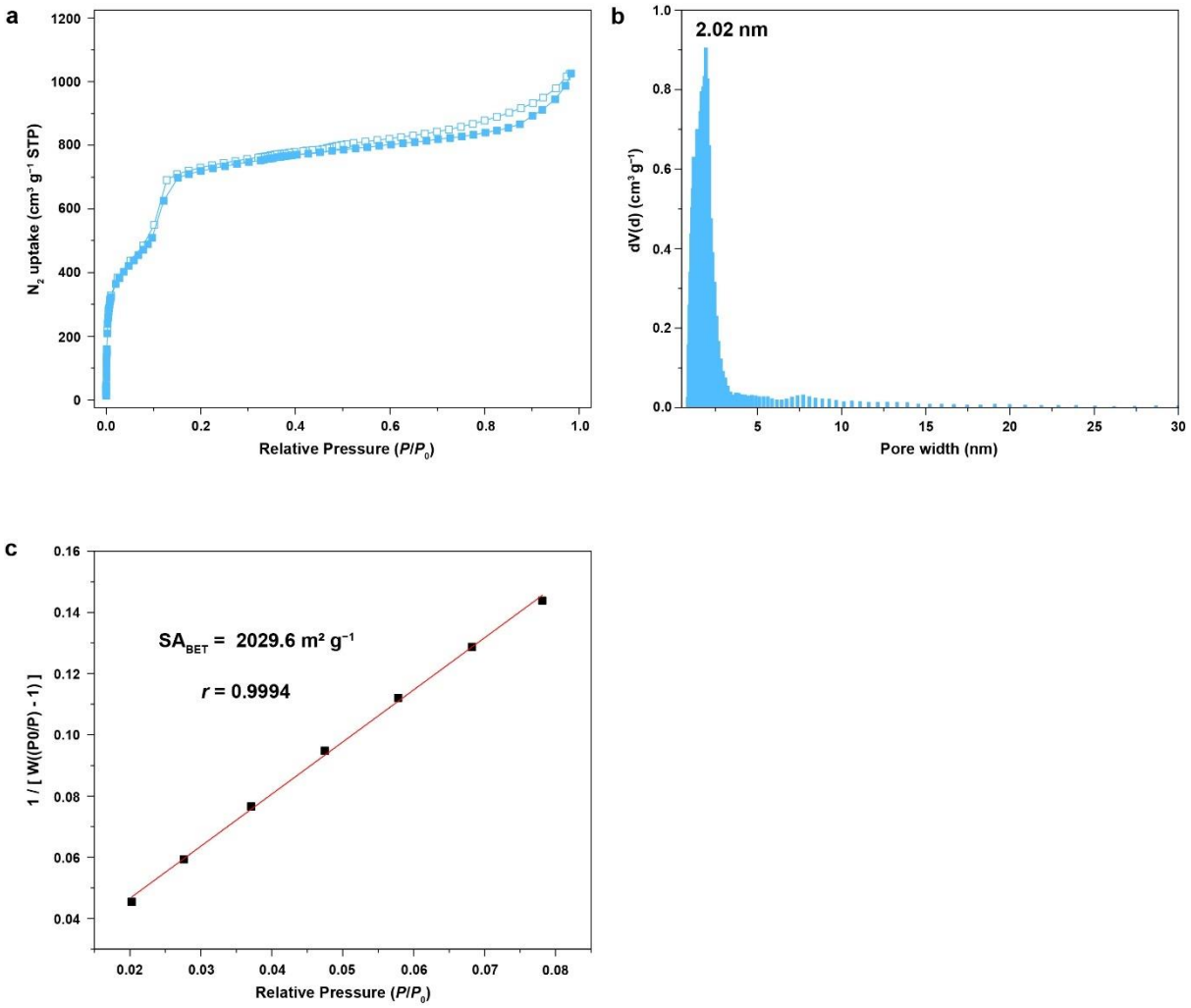

Supplementary Fig. 22 | Nitrogen sorption experiment (77 K) of Im-COF-1. a, Nitrogen sorption isotherm. **b**, Pore width distribution. **c**, Multi-point BET surface area.

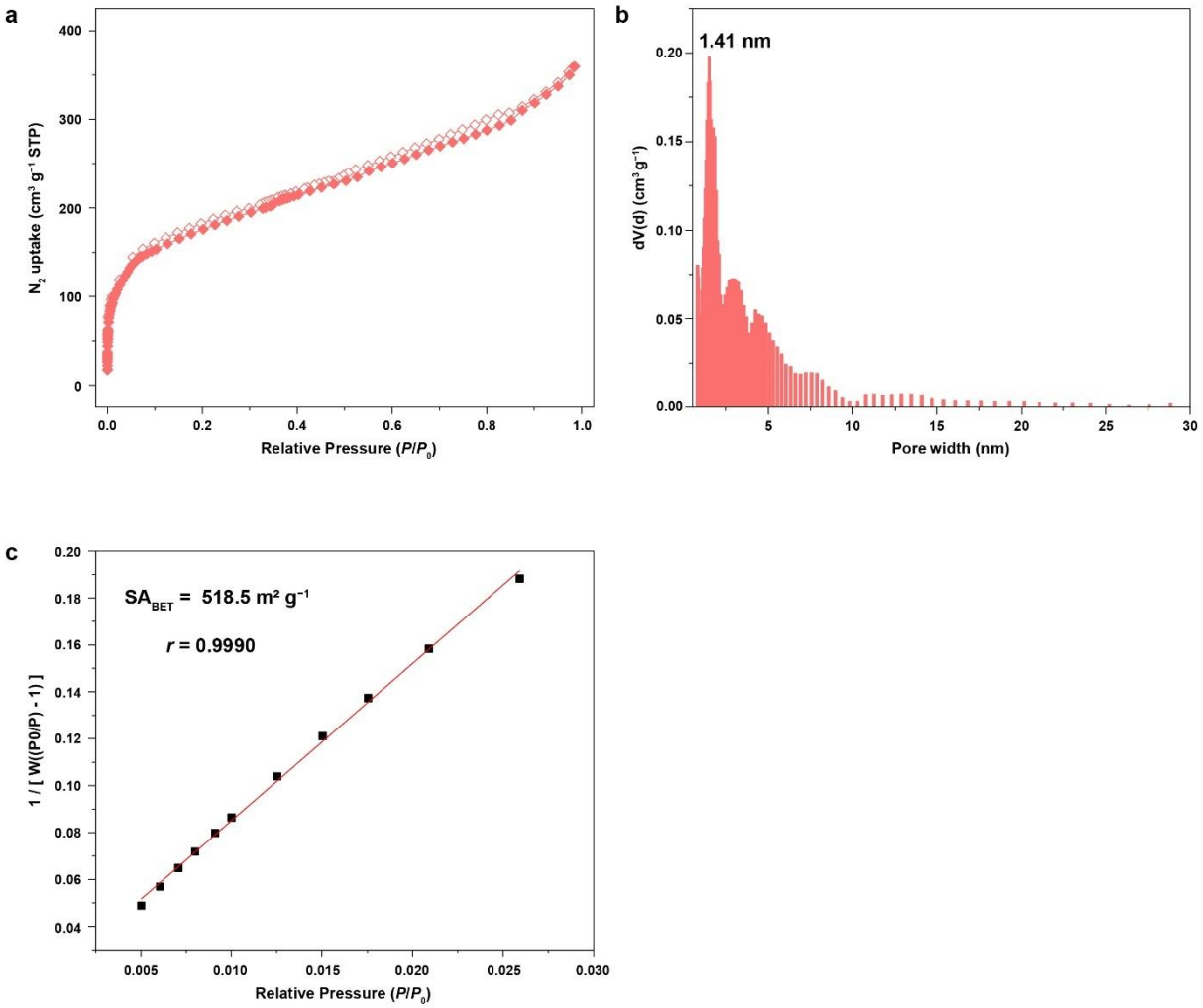

Supplementary Fig. 23 | Nitrogen sorption experiment (77 K) of IP-COF-1 synthesized via the two-step method with formalin solution as the precursor. a, Nitrogen sorption isotherm. **b**, Pore width distribution. **c**, Multi-point BET surface area.

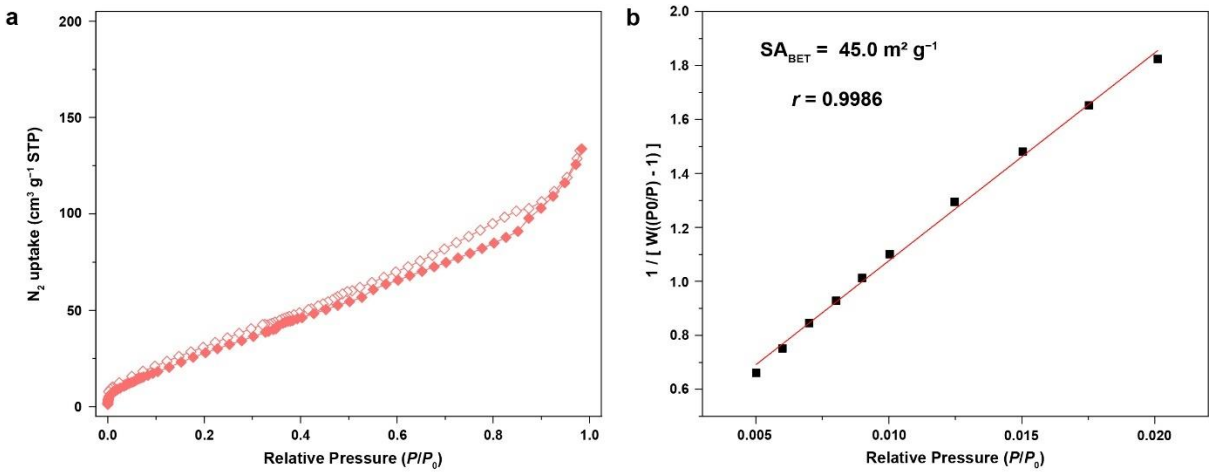

Supplementary Fig. 24 | Nitrogen sorption experiment (77 K) of IP-COF-1 synthesized via the two-step method with paraformaldehyde as the precursor. a, Nitrogen sorption isotherm. **b**, Multi-point BET surface area.

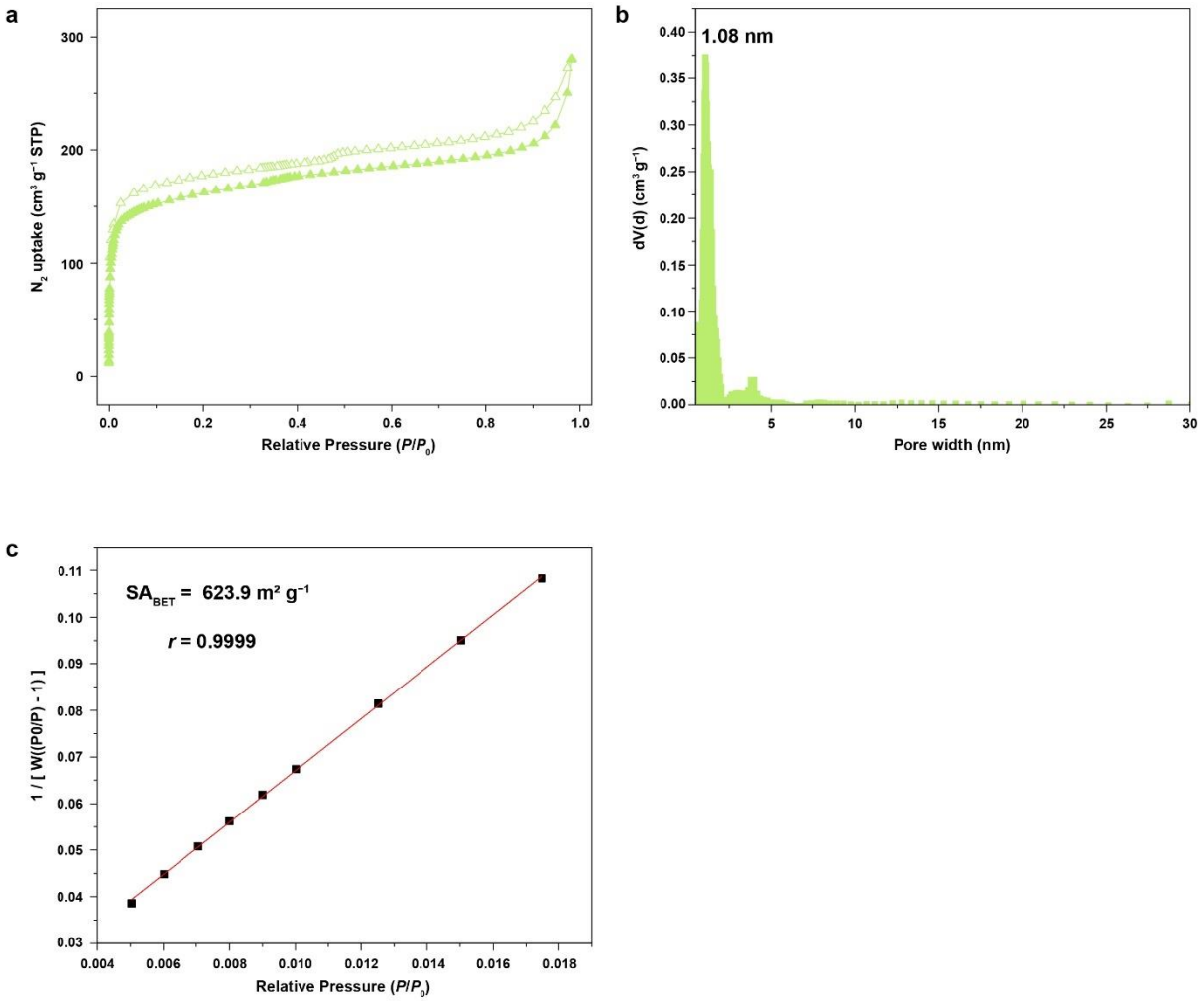

Supplementary Fig. 25 | Nitrogen sorption experiment (77 K) of Im-COF-2. a, Nitrogen sorption isotherm. **b**, Pore width distribution. **c**, Multi-point BET surface area.

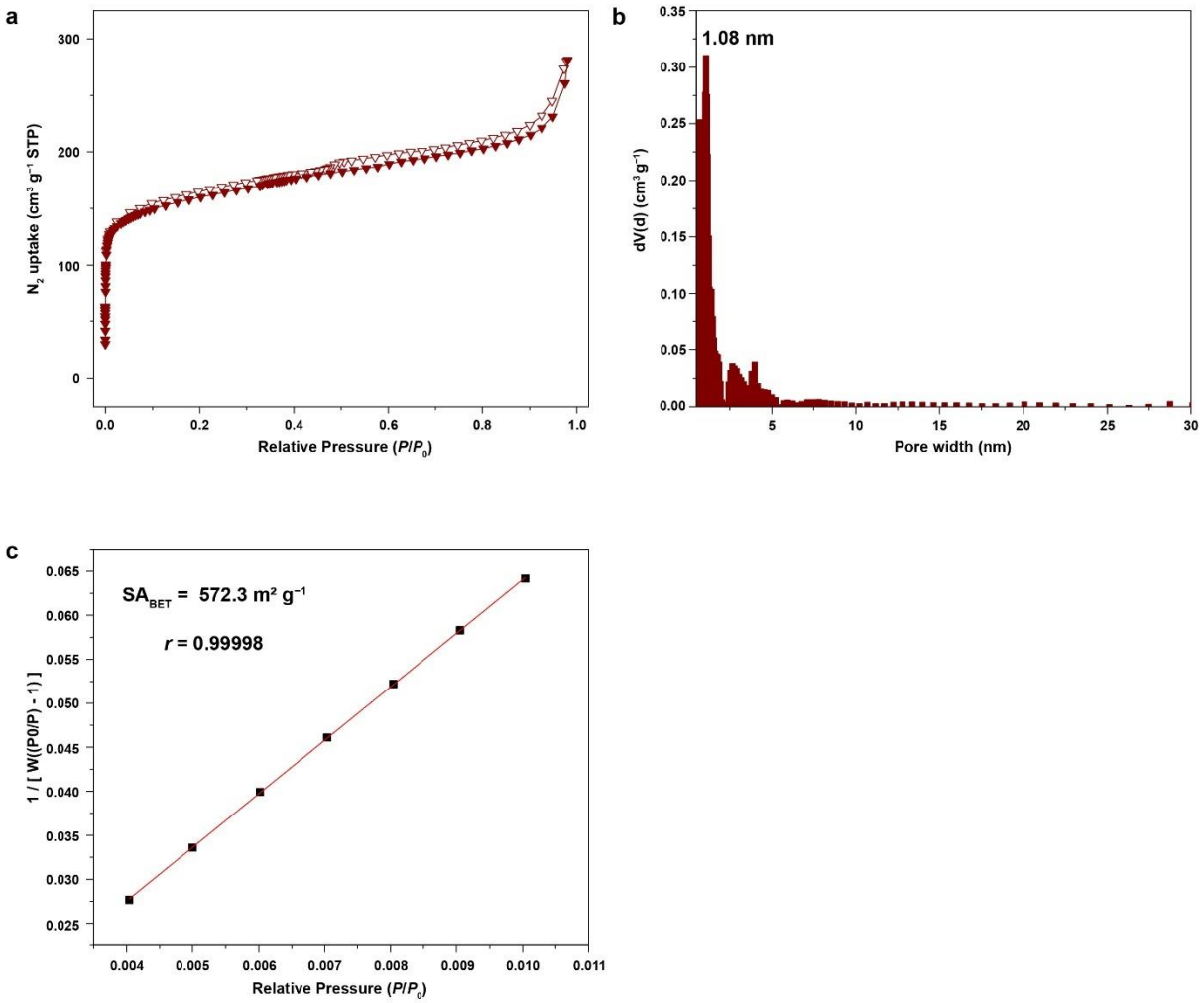

Supplementary Fig. 26 | Nitrogen sorption experiment (77 K) of IP-COF-2. a, Nitrogen sorption isotherm. **b**, Pore width distribution. **c**, Multi-point BET surface area.

Difference in pore-filling of IP-COF-1 and 2

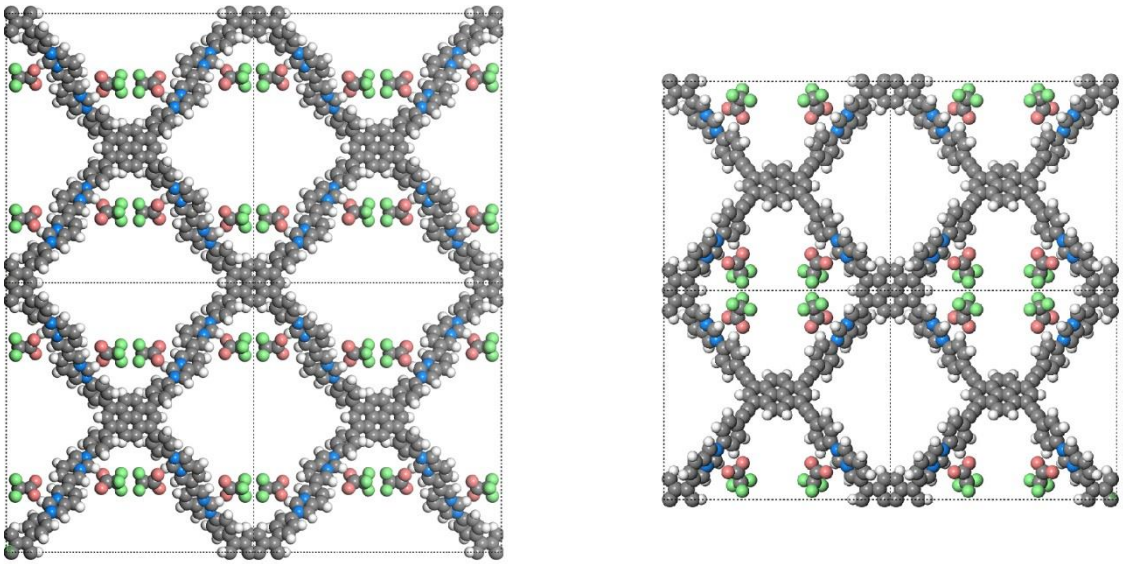

Supplementary Fig. 27 | Crystal structures of IP-COF-1 and IP-COF-2 (2 × 2 unit cells). Due to the geometry effect, only half of the pores in IP-COF-2 are occupied by trifluoroacetate anions, giving rise to the intact NLDFT pore size of 1.08 nm after imidazopyridinium linkage formation.

SEM images of COFs

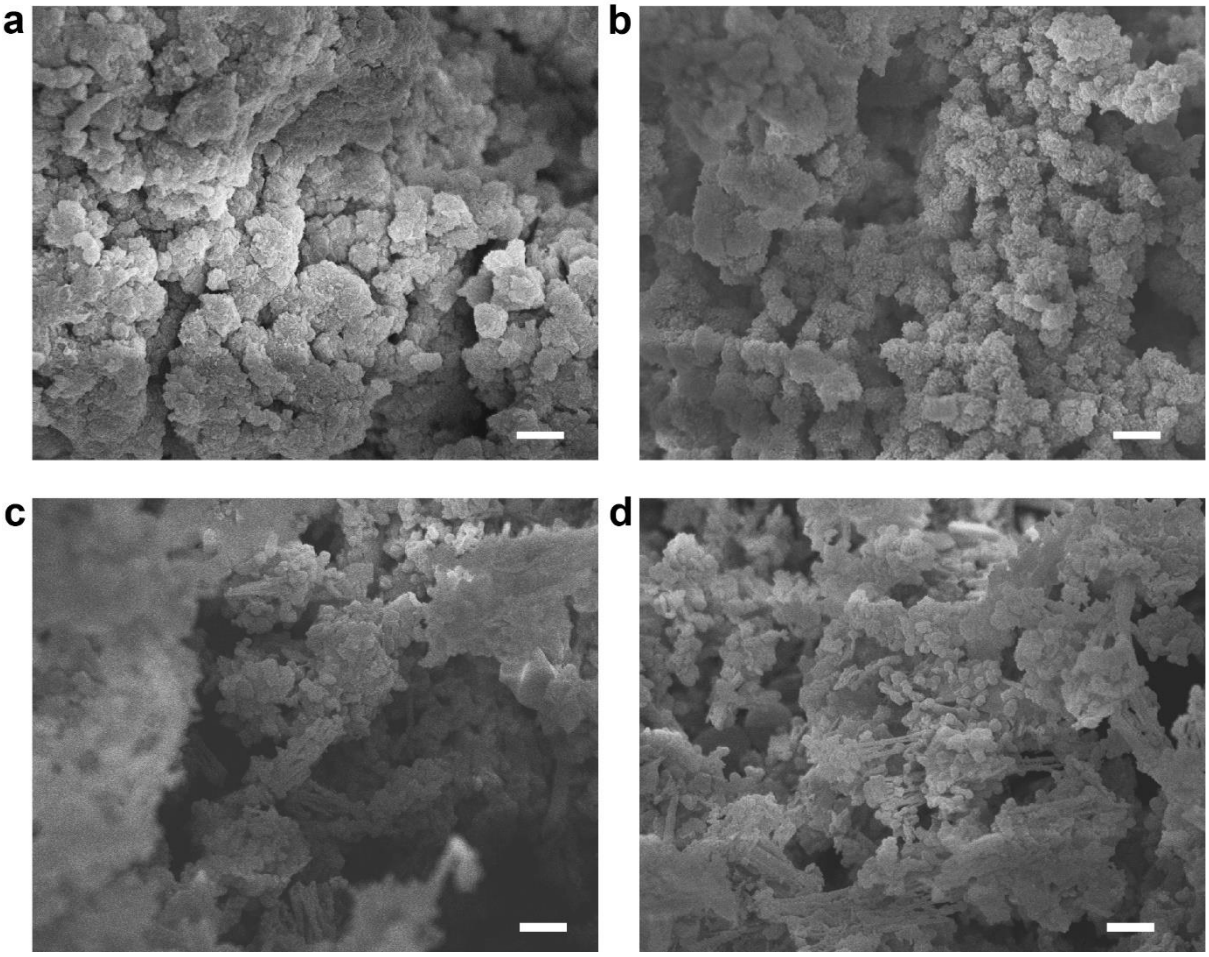

Supplementary Fig. 28 | SEM images of COFs. a, Im-COF-1. **b**, IP-COF-1. **c**, Im-COF-2. **d**, IP-COF-2 (Scale bar: 1 μm).

TEM images of Im-COFs

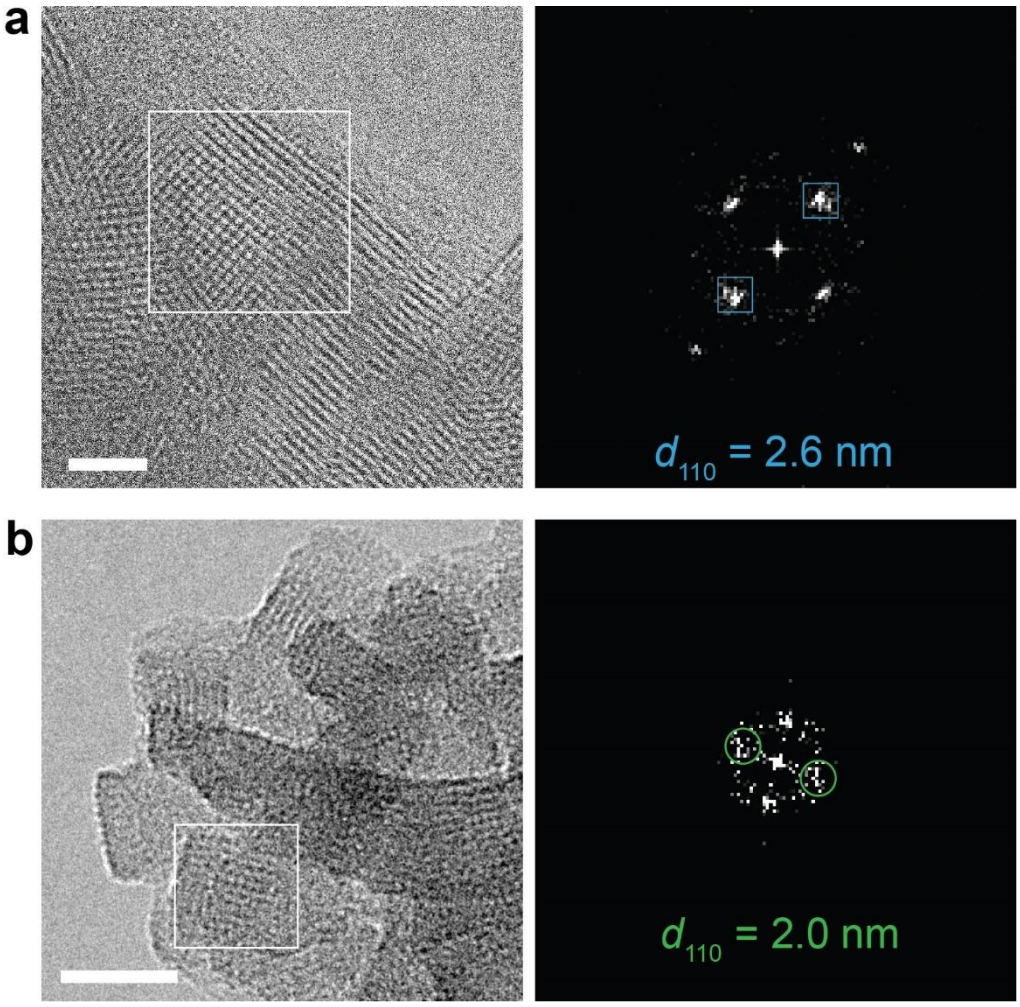

Supplementary Fig. 29 | TEM image of Im-COFs. a, TEM image of Im-COF-1 and its selected-area FFT. **b**, TEM image of Im-COF-2 and its selected-area FFT (Scale bar: 20 nm).

TEM images of AB-stacked IP-COF-2

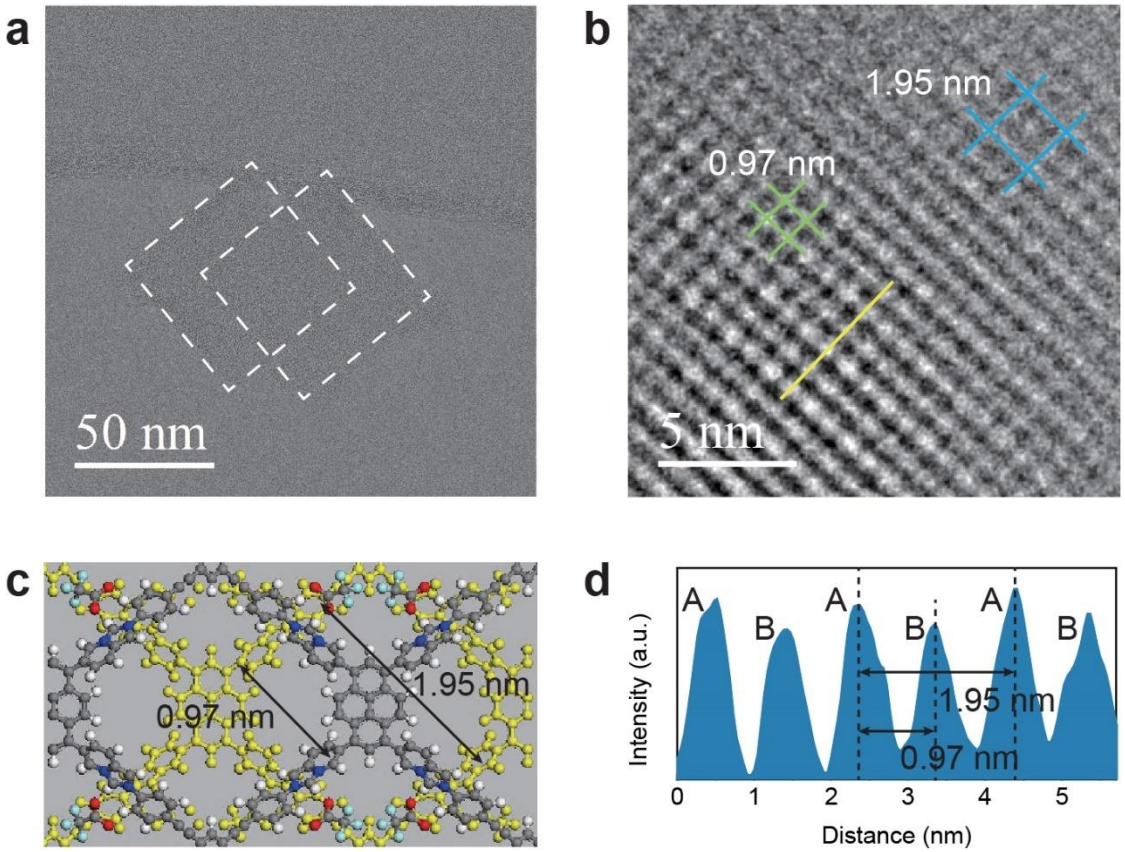

Supplementary Fig. 30 | Cryo-TEM image of AB-stacked IP-COF-2. a, Low magnification Cryo-TEM image of the stacked IP-COF-2 layers. The white dashed squares highlight individual flakes with rectangular shape. **b**, High-resolution lattice fringes image magnified from a selected area in **a**, showing two kinds of lattice periodicities, in which the spacing of 1.95 nm marked by blue short lines corresponds to the (110) lattice facet of IP-COF-2 viewed along [001] zone axis, and the halved interplanar spacing (0.97 nm) originates from the AB stacking of two IP-COF-2 layers. **c**, Schematic atomic structure of AB stacking in IP-COF-2. The second layer is in yellow colour. **d**, Line intensity profiles along the highlighted yellow lines in **b**, exhibiting two different phase intensities, corresponding to different layers of COF backbones in the upper and lower layers.

High-resolution AFM

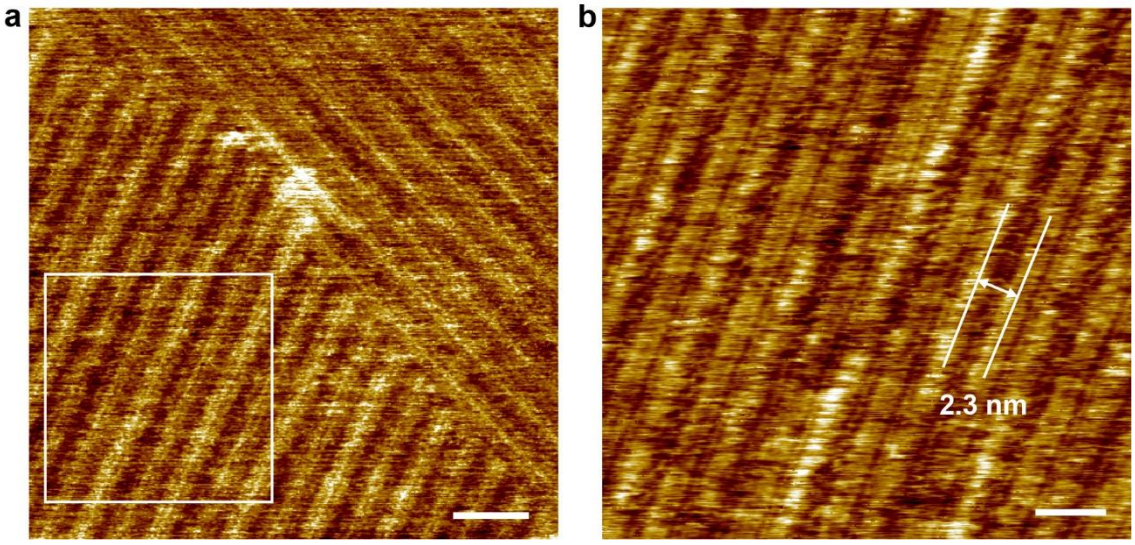

Supplementary Fig. 31 | High resolution AFM of IP-COF-1 on HOPG (Scale bar: **a**, 10 nm. **b**, 4 nm).

Single-crystal structure of model compound

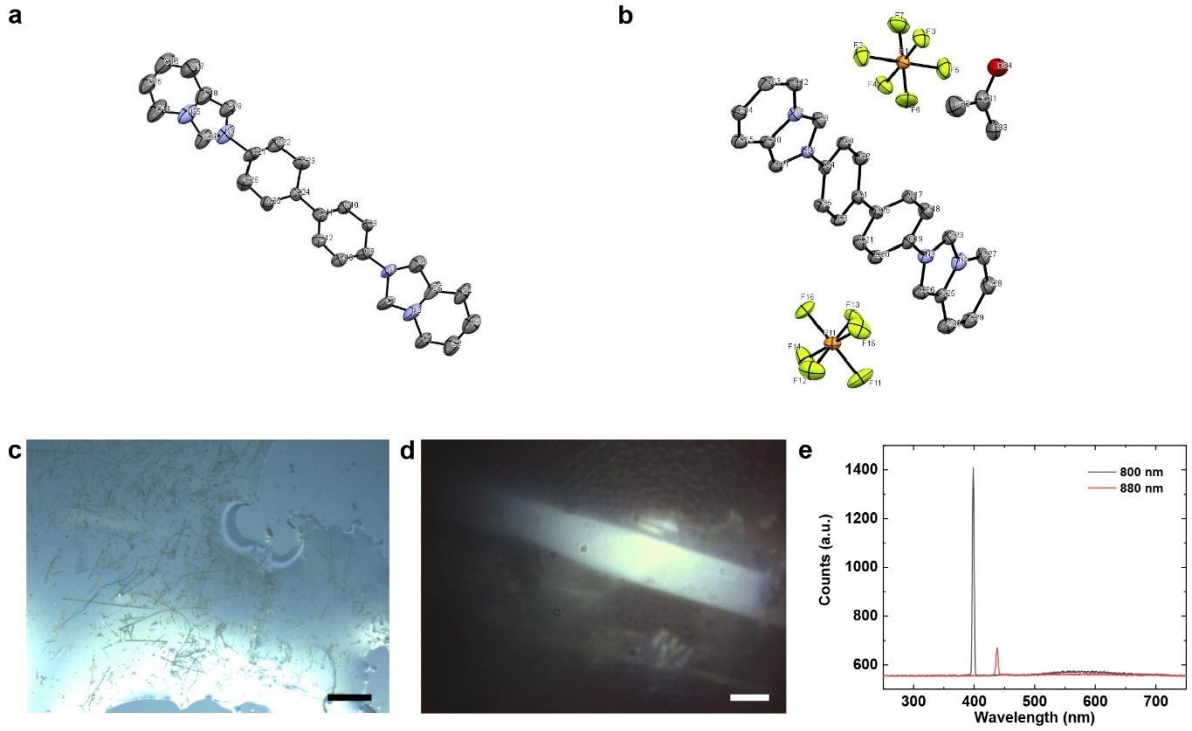

Supplementary Fig. 32 | Characterization of the single-crystal structure of the COF model compounds. a, Single-crystal structure of the COF model compound with trifluoroacetate anion (IP-model-1); the solvent and anion have been masked *via* SQUEEZE due to the high degree of disordering. **b**, Single-crystal structure of the COF model compound with hexafluorophosphate anion (IP-model-2); the strong disorder of fluoride anion is hidden for illustration purposes; hexafluorophosphate counter anion was utilized to improve the crystal quality of the model compound. **c**, Crystals of the COF model compound with trifluoroacetate anion dispersed in paratone oil for crystal picking (scale bar: 200 μm). **d**, Crystal of the COF model compound with trifluoroacetate anion in paratone oil for second harmonic generation (SHG) analysis (scale bar: 50 μm). **e**, plot of SHG intensity using pump laser with a wavelength of 800 nm and 880 nm. The slight bump centred at around 580 nm originate from the ambient lighting.

Note: In parallel to the ^{1}H NMR, ^{13}C NMR and accurate mass characterization, we collected the single-crystal X-ray data of the COF model compound to confirm the chemical structure, all of which are to verify the viability of building imidazopyridinium linkages in COFs. The COF model compound with trifluoroacetate counteranion, IP-model-1, exhibits high degree of disordering in the trifluoroacetate anions, which are therefore masked *via* SQUEEZE. This gives rise to B-level alerts in the .cif file of IP-model-1. In addition, Second Harmonic Generation (SHG) experiment was conducted on the IP-model-1 crystals, proving the absence of inversion centre. Therefore, we confirm the crystal structure of IP-model-1 exhibits a space group of *Cc* with an R1 value of 7%. To improve the crystal quality, we also attempted to crystallize the COF model compound with hexafluorophosphate conteranions, IP-model-2. The .cif file of IP-model-2 exhibits no A- or B-level alerts, despite the disorder of one PF_6^- which gives rise to a penalty in the form of a R1 value of 11%. Overall, we have demonstrated that the successful conversion of imidazopyridinium cations using a very similar synthetic condition to IP-COFs.

^{1}H NMR spectrum of the COF model compound

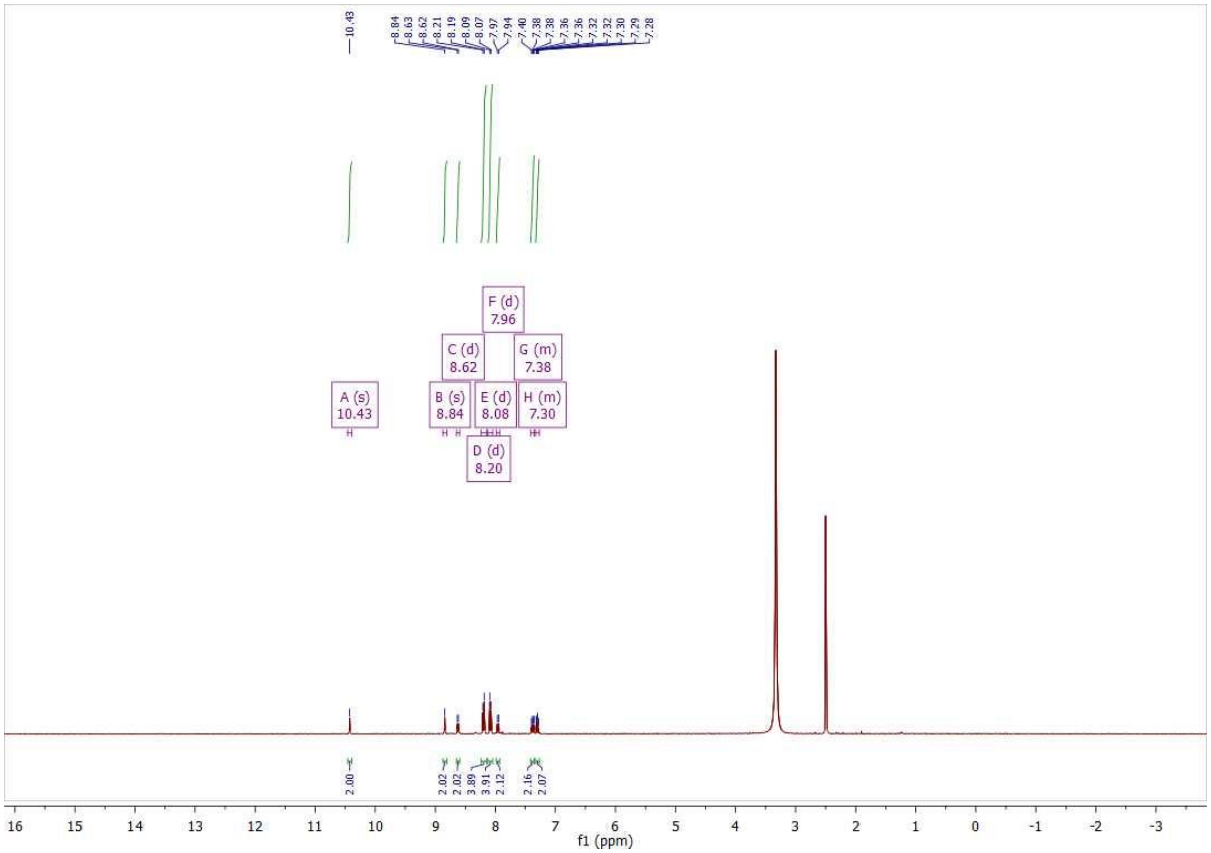

Supplementary Fig. 33 | ^{1}H NMR spectrum of the COF model compound (IP-model-1) in DMSO-*d*6.

^{13}C NMR spectrum of the COF model compound

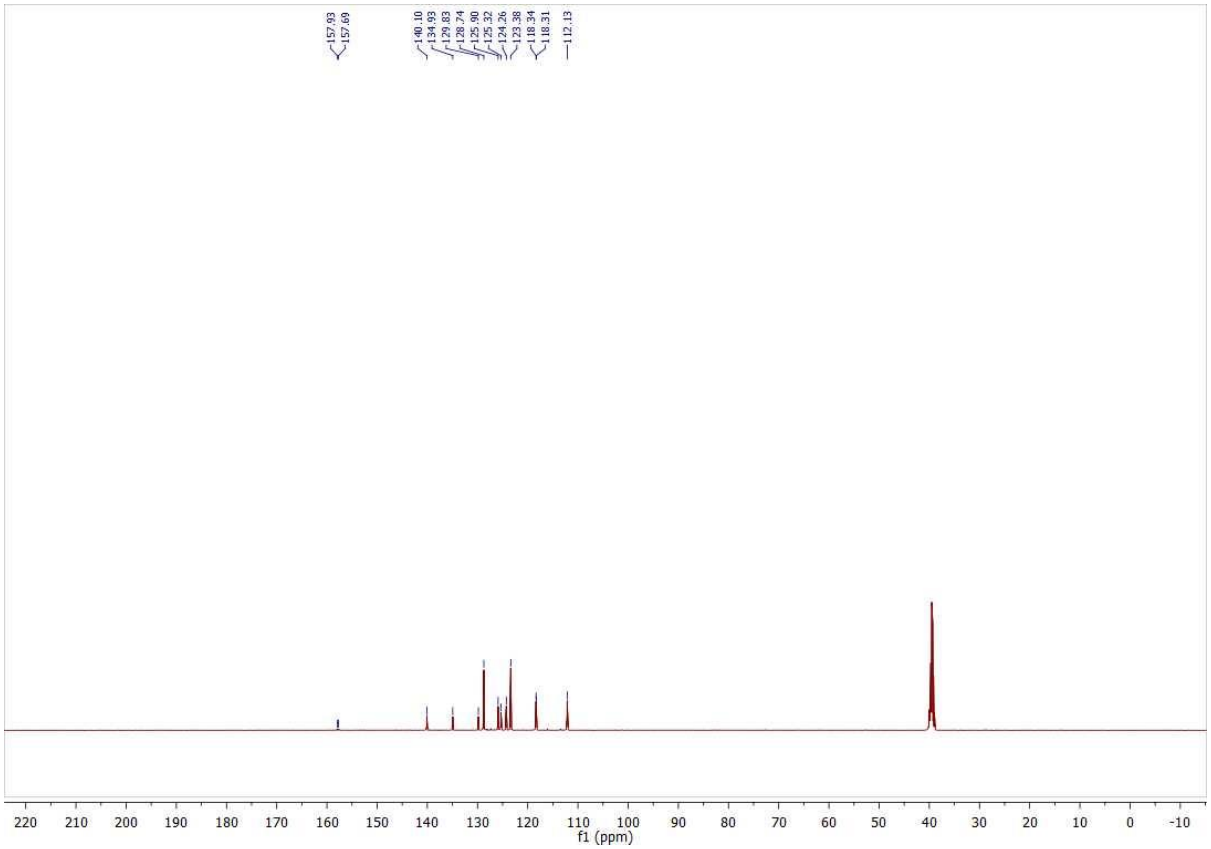

Supplementary Fig. 34 | ^{13}C NMR spectrum of the model compound (IP-model-1) in DMSO-*d*6.

Li-S battery performance

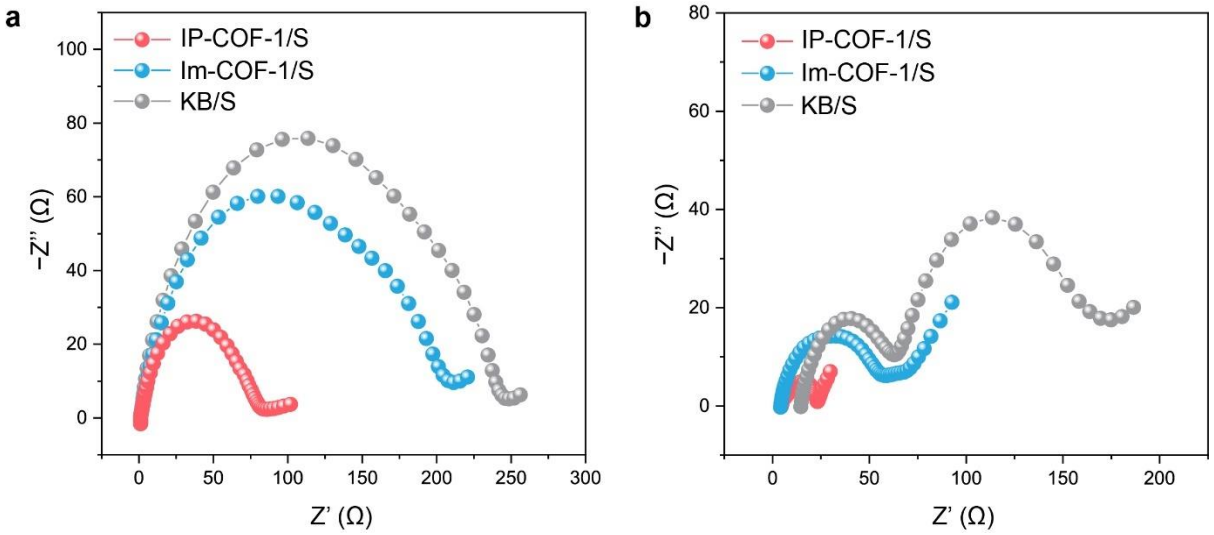

Supplementary Fig. 35 | EIS Nyquist plots of IP-COF-1, Im-COF-1, and KB cathodes **a**, before and **b**, after 100 cycles at 0.2 C.

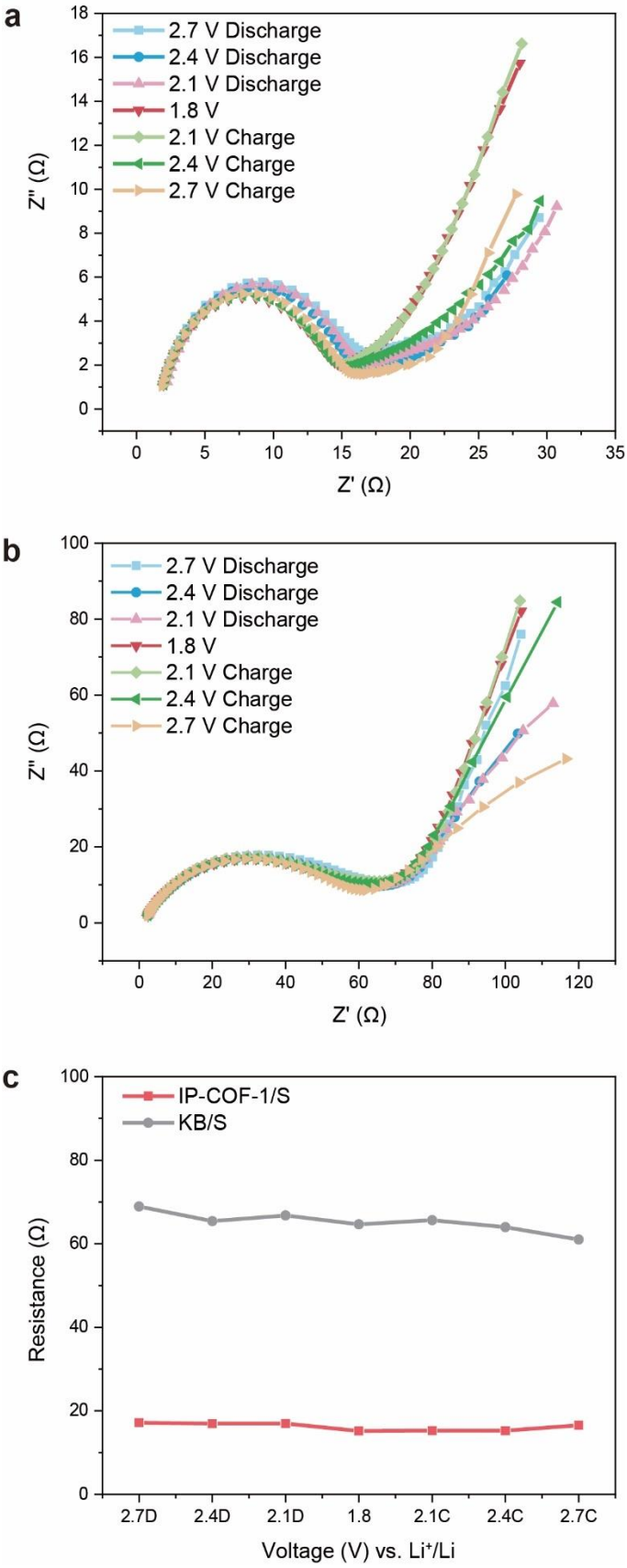

Supplementary Fig. 36 | EIS Nyquist plots of cathodes at different charge-discharge stages. a, IP-COF-1/S cathode. **b**, KB/S cathode. **c**, Comparison of resistance between the two cells.

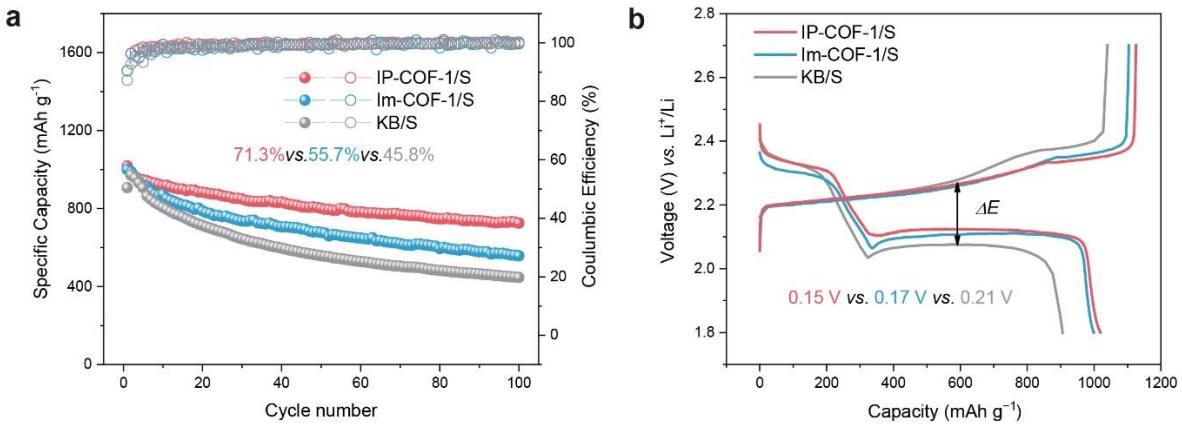

Supplementary Fig. 37 | Cycling performance of Li-S batteries. a, Cycling performance of batteries with IP-COF-1/S, Im-COF-1/S, and KB/S cathodes at 0.2 C. **b**, Corresponding galvanostatic charge/discharge profiles of IP-COF-1/S, Im-COF-1/S, and KB/S electrodes at 0.2 C.

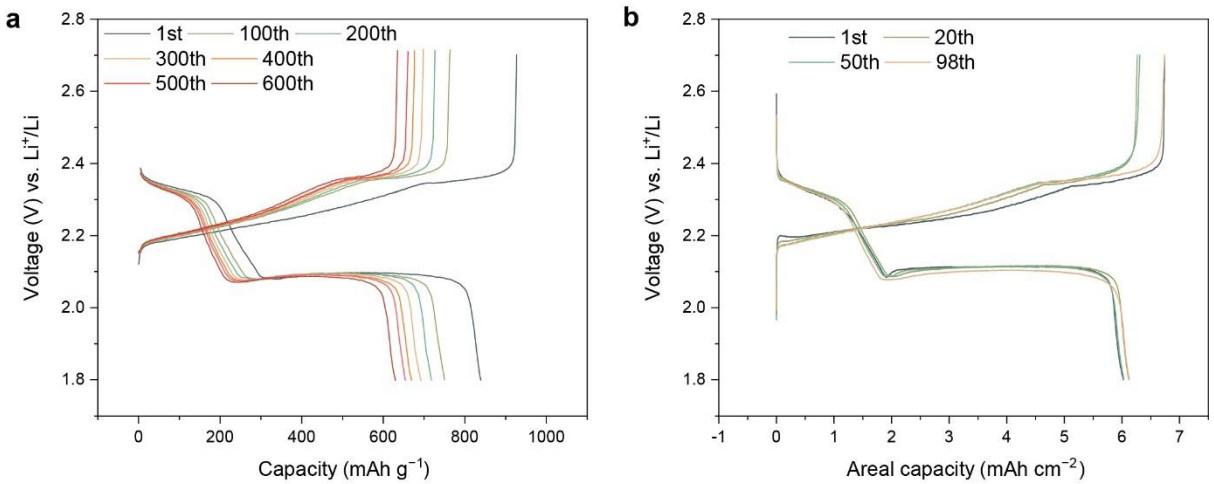

Supplementary Fig. 38 | Galvanostatic charge/discharge profiles of Li-S batteries with IP-COF-1/S cathode. a, Galvanostatic charge/discharge profiles correspond to cycling performance at 0.2 C. **b**, Galvanostatic charge/discharge profiles correspond to cycling performance of high S loading (~9 mg cm^{-2}) battery at 0.05 C.

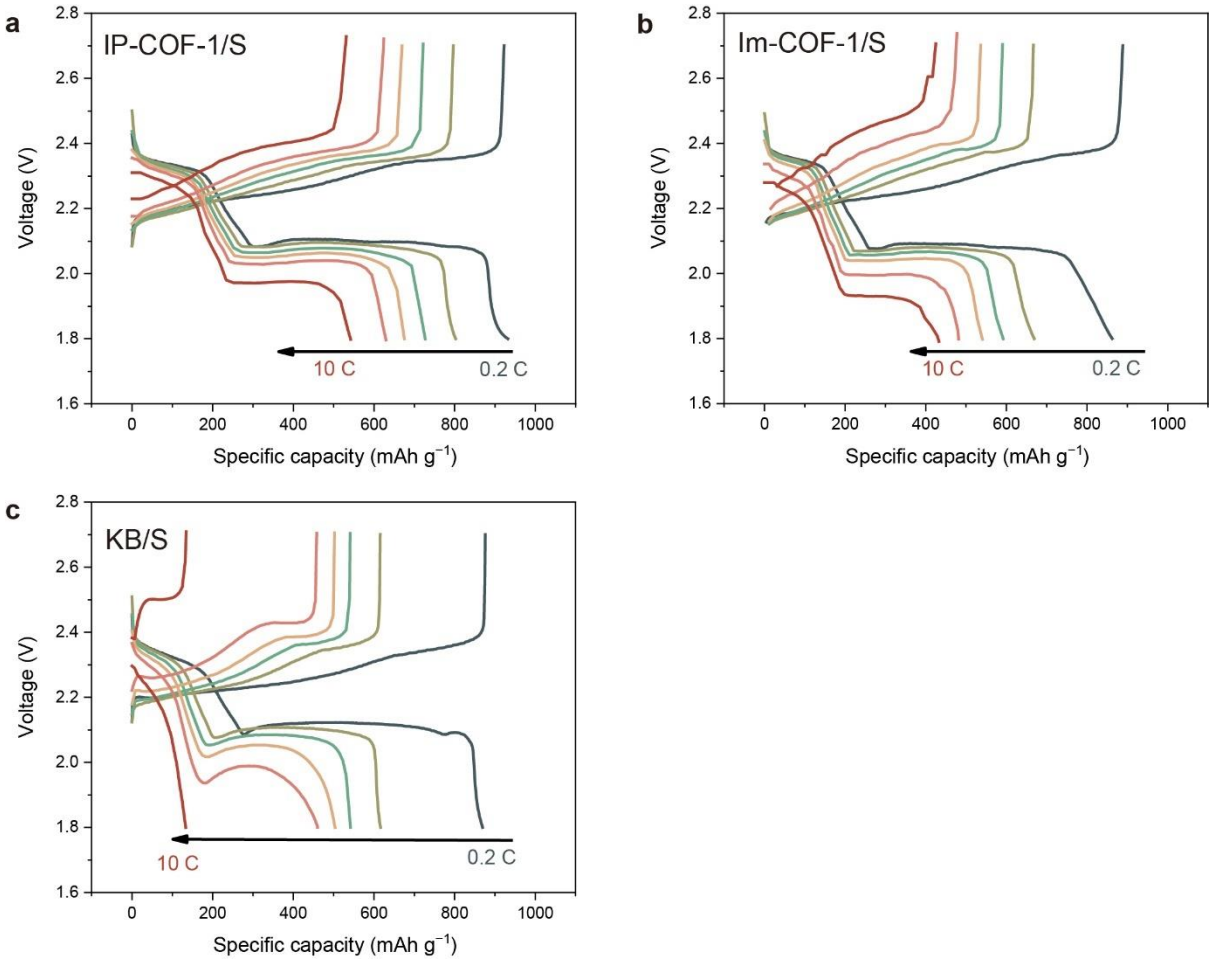

Supplementary Fig. 39 | Galvanostatic charge/discharge profiles. a, IP-COF-1/S, **b**, Im-COF-1/S, and **c**, KB/S electrodes at different current density.

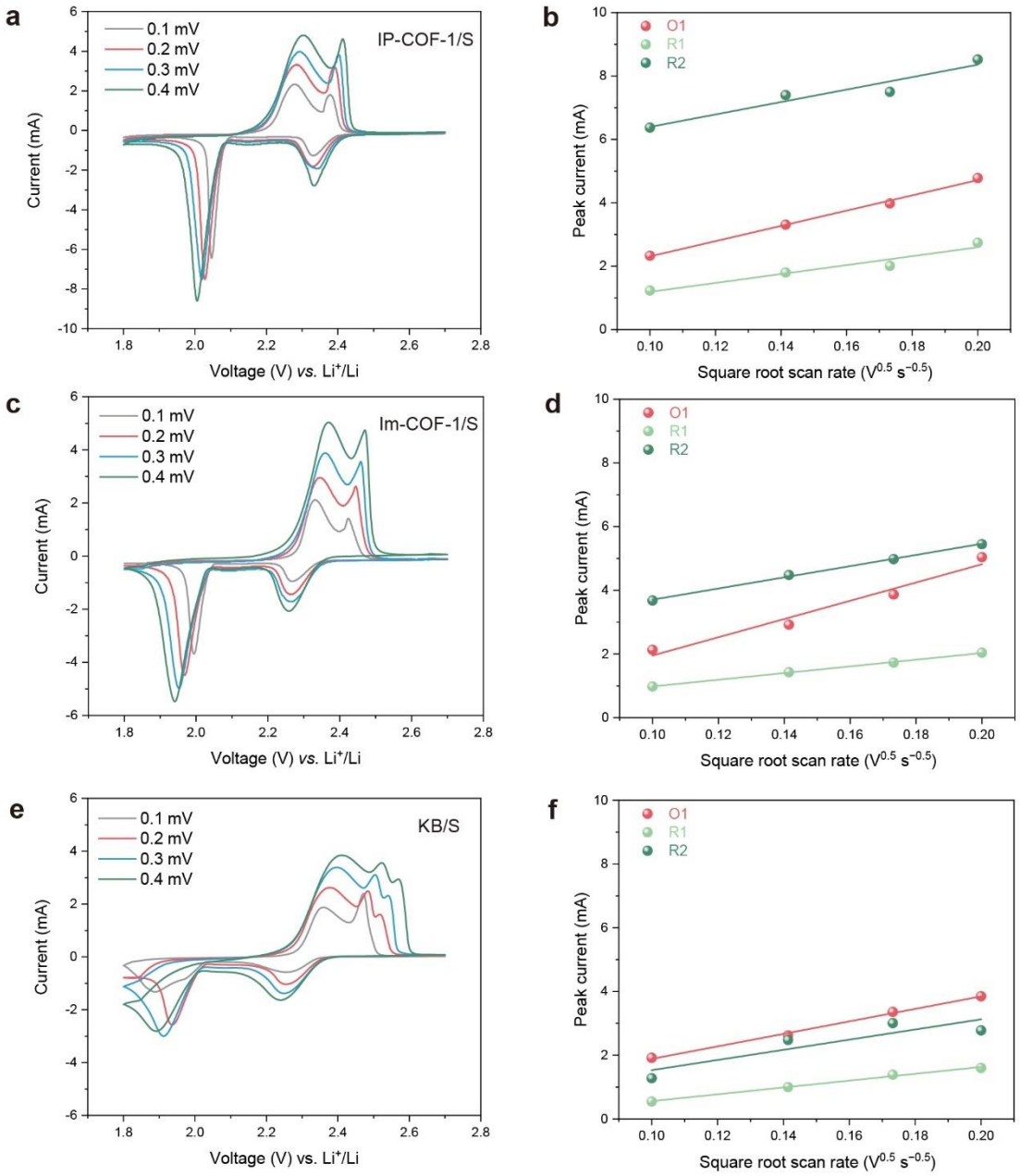

Supplementary Fig. 40 | Probing the redox kinetics of the Li-S batteries with various cathode. a-c, CV curves of IP-COF-1/S, Im-COF-1/S, and KB/S cathodes under different scanning rates ranging from 0.1 to 0.4 mV s^{-1} between 1.8 and 2.7 V (vs. Li^+/Li). **d-f**, The value of $I_P/V^{0.5}$ from that represent Li-ion diffusion ability of anodic oxidation process (I_A), first cathodic reduction process (I_{C1}), and second cathodic reduction process (I_{C2}), respectively.

Confirming the sulfur content in the cathodes

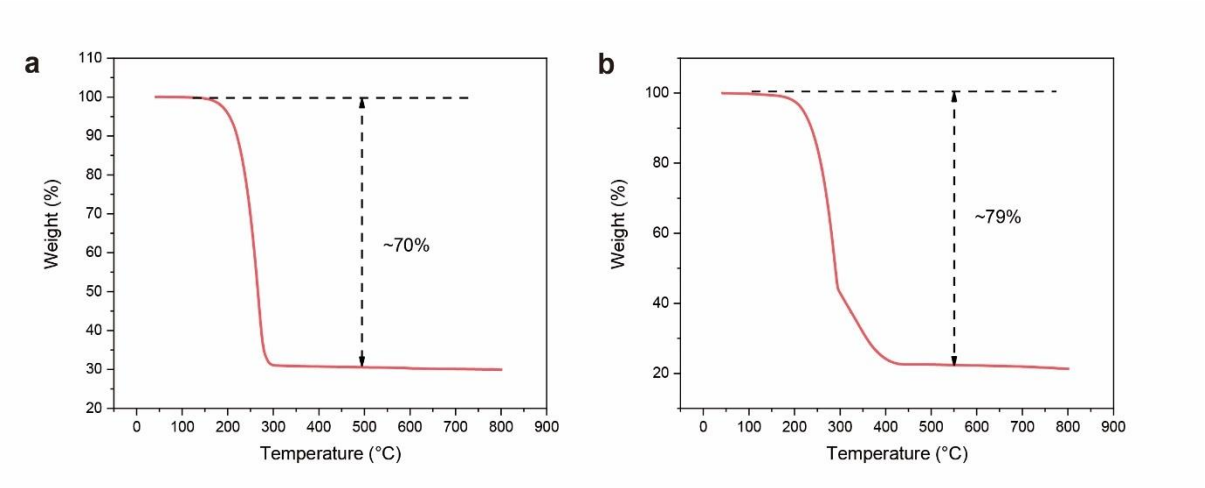

Supplementary Fig. 41 | TGA profiles of IP-COF-1/S composites with different sulfur loading. a, Low sulfur loading (~1 mg cm^{-2}). **b**, High sulfur loading (~9 mg cm^{-2}).

XPS of the electrodes before battery cycling

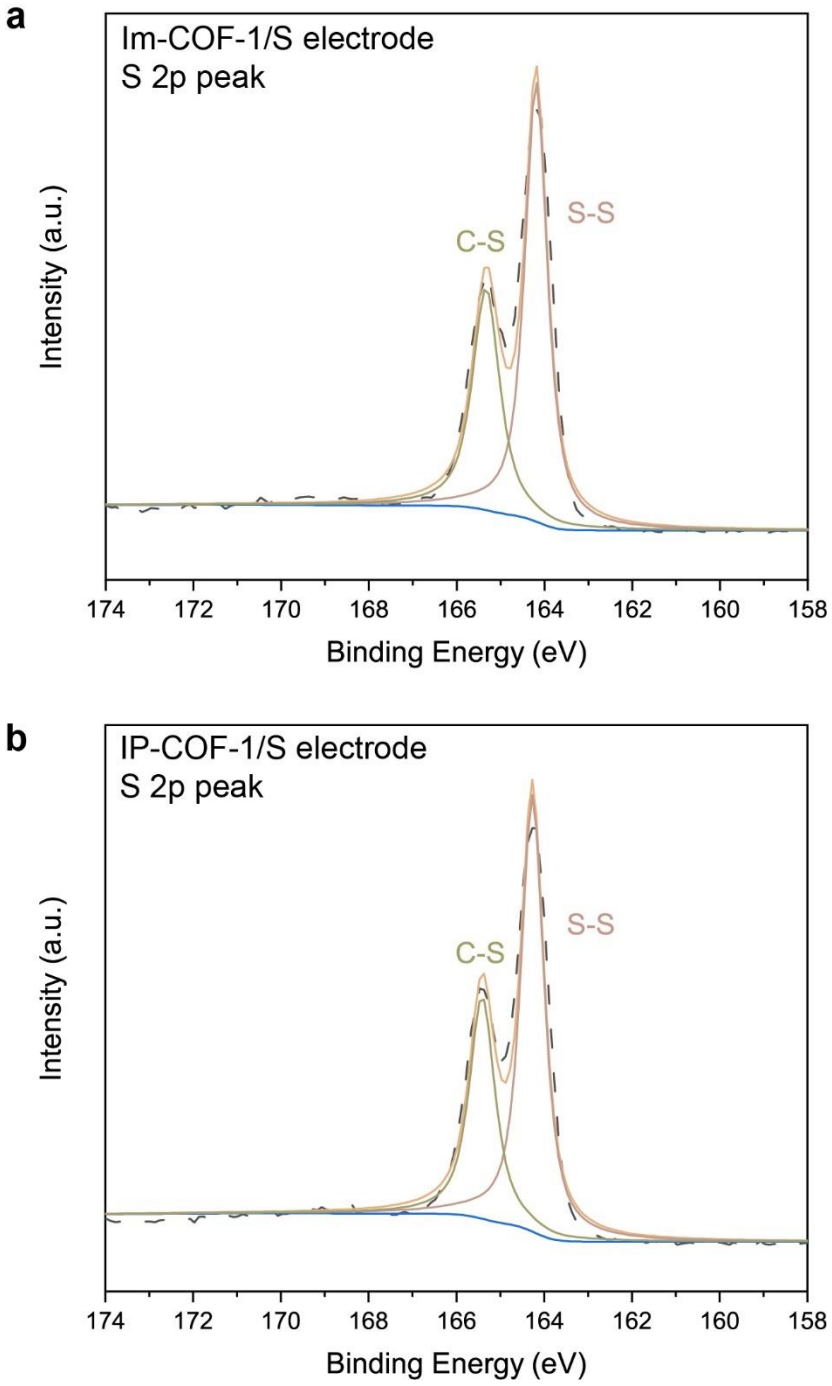

Supplementary Fig. 42 | XPS spectra of the cathodes before battery cycling. a, Im-COF-1/S. **b**, IP-COF-1/S.

CV curve of IP-COF-1

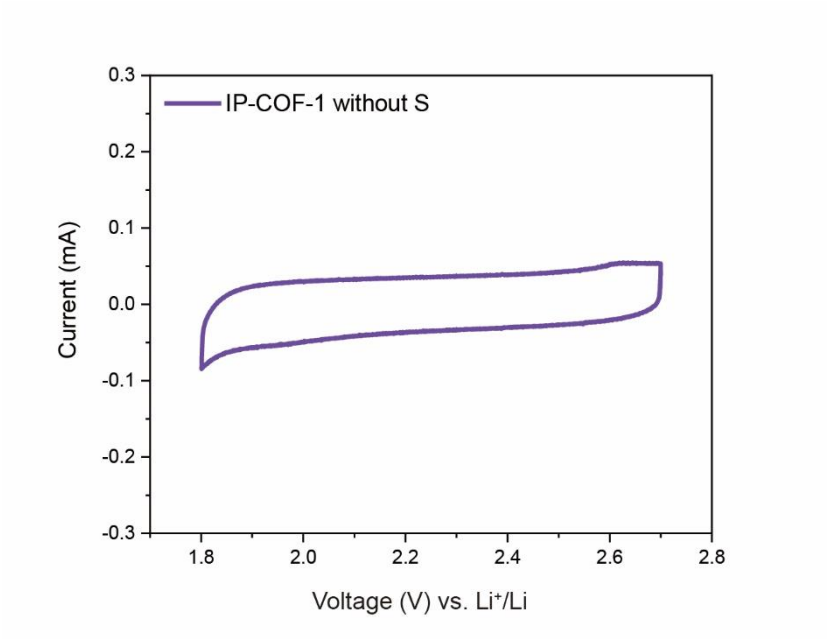

Supplementary Fig. 43 | CV curve of IP-COF-1 cathode without sulfur at a scan rate of 1 mV s^{-1} in the voltage range of 1.8 V to 2.7 V.

Microscopic imaging of the Li-S battery components

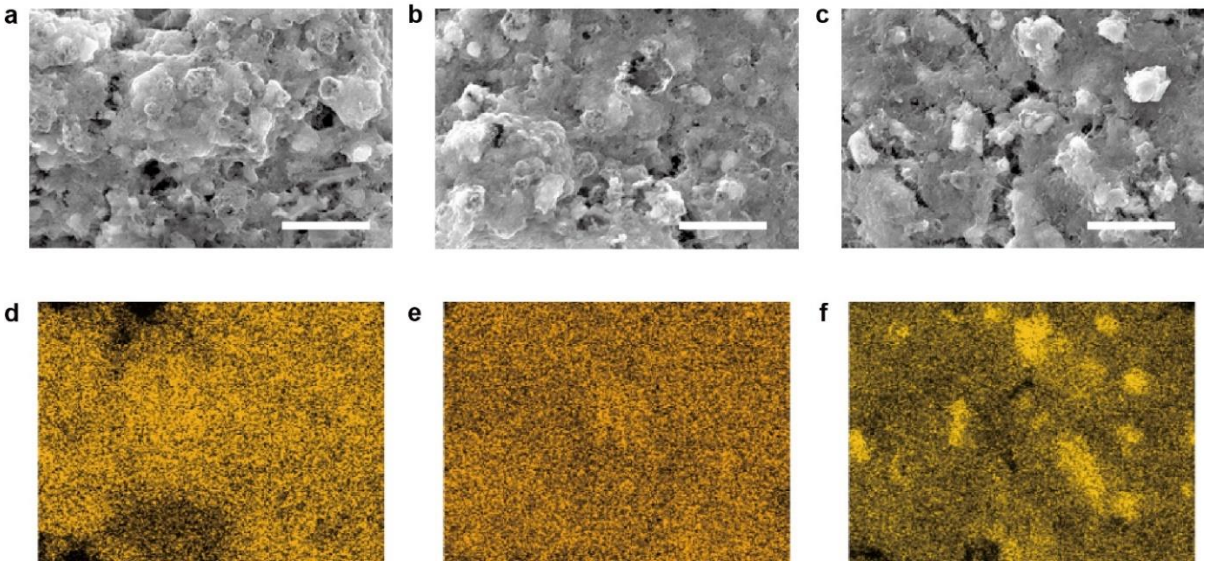

Supplementary Fig. 44 | SEM images of the cathodes before battery cycling and corresponding element sulfur EDS mapping. a and **d**, IP-COF-1 cell. **b** and **e**, Im-COF-1 cell. **c** and **f**, KB cell (scale bar: 20 μm).

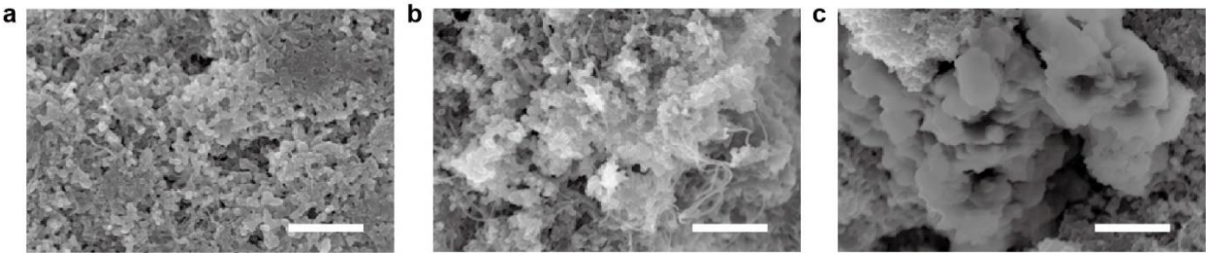

Supplementary Fig. 45 | SEM images of the cathodes after the 1st discharge. a, IP-COF-1 cell. **b**, Im-COF-1 cell. **c**, KB cell (scale bar: 1 μm).

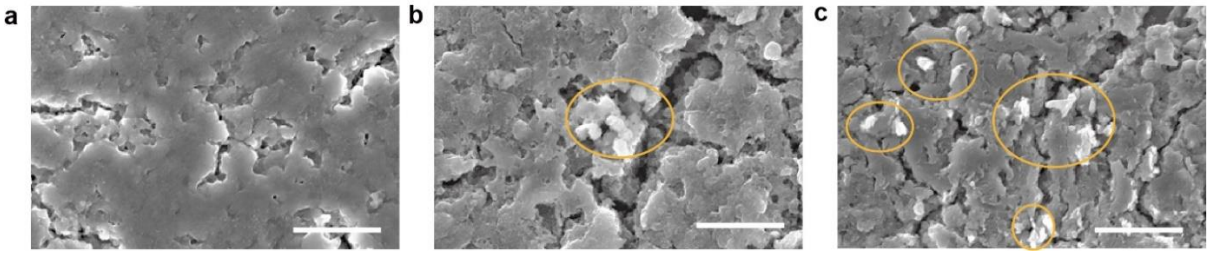

Supplementary Fig. 46 | SEM images of cathodes after 100 cycles at 1 C. a, IP-COF-1 cell. **b**, Im-COF-1 cell. **c**, KB cell (scale bar: 20 μm). The Li_2S residues after recharging are highlighted in yellow circles.

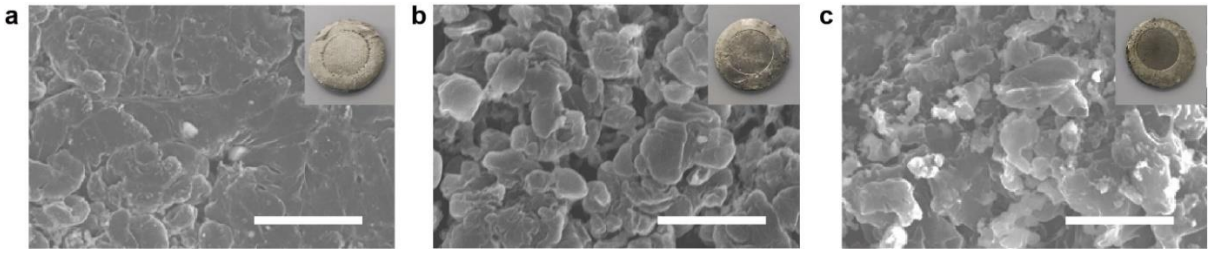

Supplementary Fig. 47 | SEM images and photo images of the Li anodes after 100 cycles at 1 C (1 C = 1675 mA g^{-1}). a, IP-COF-1/S cell. **b**, Im-COF-1/S cell. **c**, KB/S cell (scale bar: 20 μm).

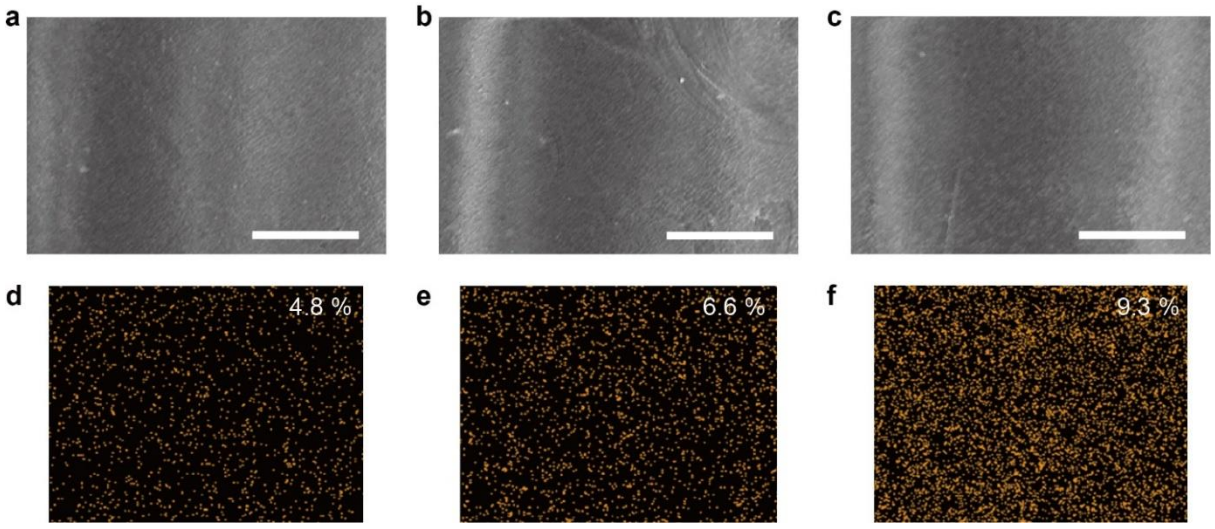

Supplementary Fig. 48 | SEM images and corresponding elemental sulfur EDS mapping of the separators (cathode side) after 100 cycles at 1 C (1 C = 1675 mA g^{-1}). **a** and **d**, IP-COF-1 cell. **b** and **e**, Im-COF-1 cell. **c** and **f**, KB cell (scale bar: 20 μm). The weight percentage of sulfur content is shown in the EDS mapping.

Polysulfide adsorption test

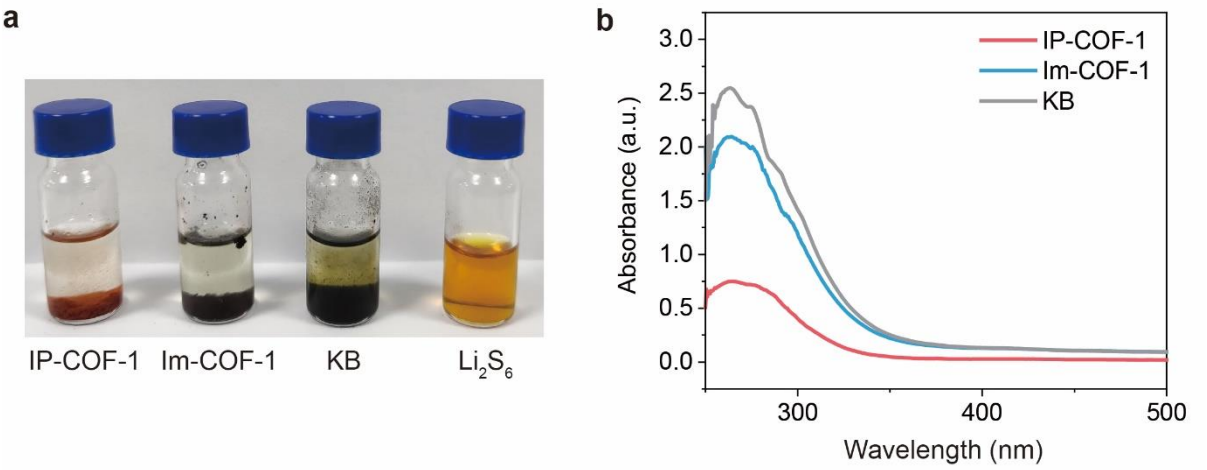

Supplementary Fig. 49 | Adsorption test of polysulfides (Li_2S_6) using IP-COF-1, Im-COF-1 and KB. **a**, Photo image of the adsorbent-Li_2S_6 mixtures after standing for 12 h. **b**, UV-vis absorption spectra of the Li_2S_6 solutions 12 h after IP-COF1, Im-COF-1 and KB was added, respectively.

Electrolyte wettability test

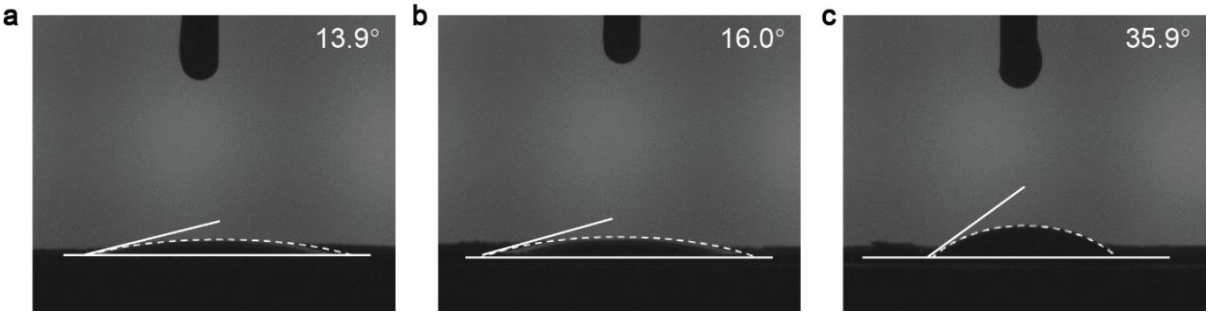

Supplementary Fig. 50 | Contact angle of electrolyte on various cathodes. **a**, IP-COF-1/S cathode, **b**, Im-COF-1/S cathode. **c**, KB/S cathode.

NMR spectra

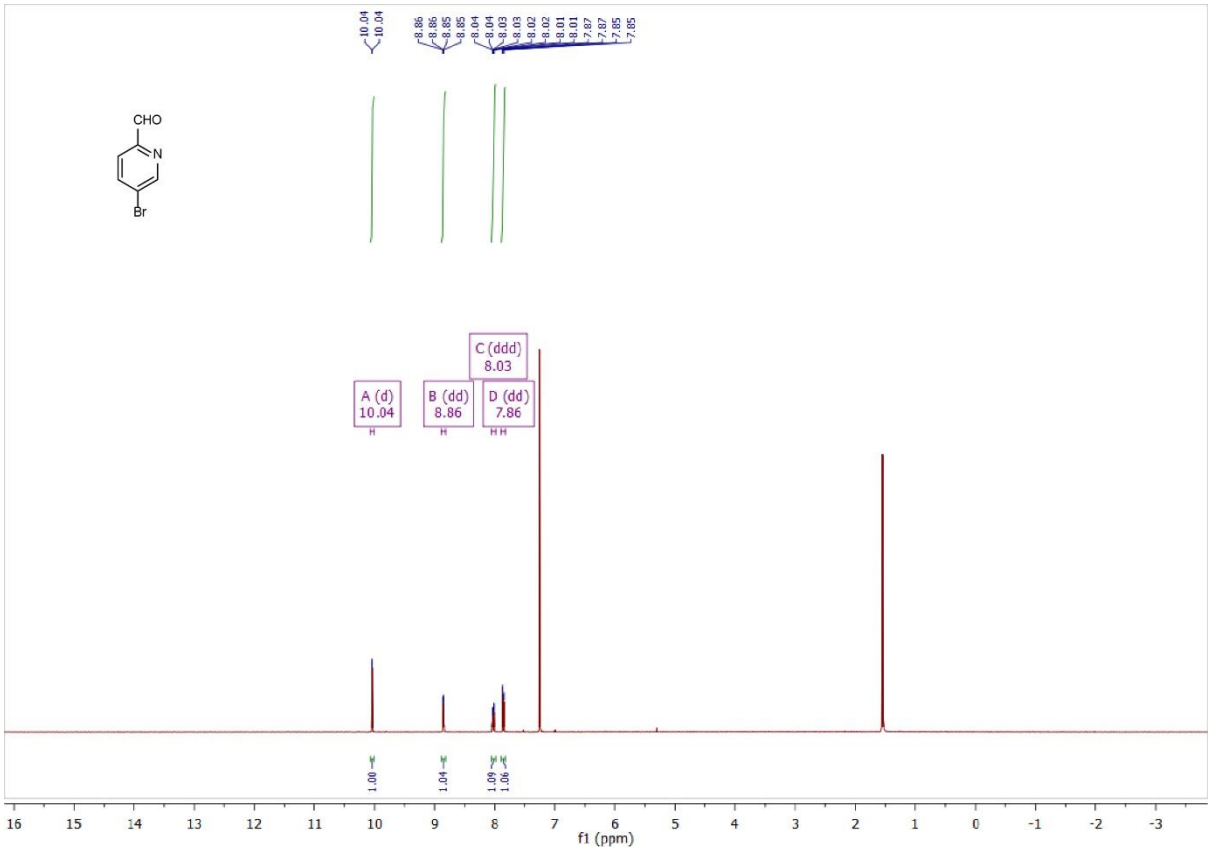

^{1}H NMR spectrum of 5-bromopicolinaldehyde (400 MHz, $CDCl_3$).

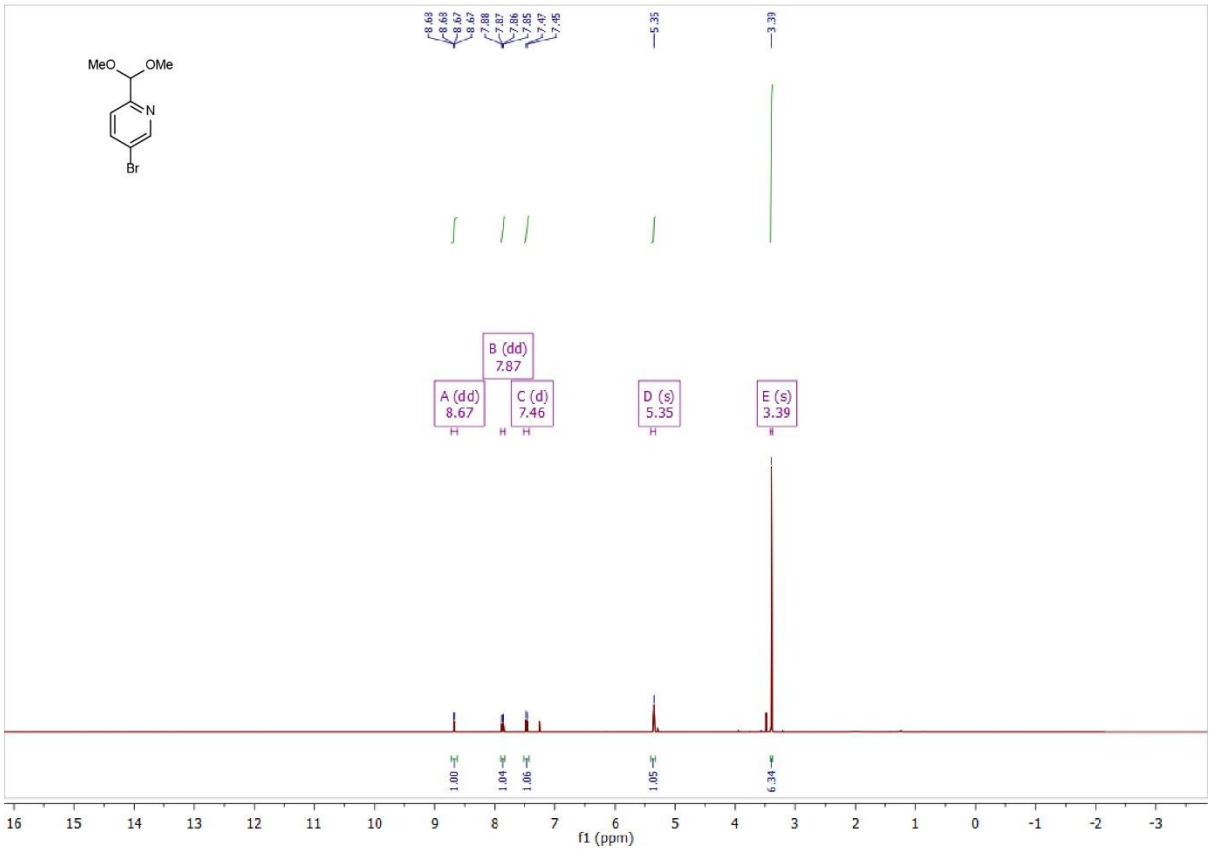

^{1}H NMR spectrum of 5-bromo-2-(dimethoxymethyl)pyridine (400 MHz, $CDCl_3$).

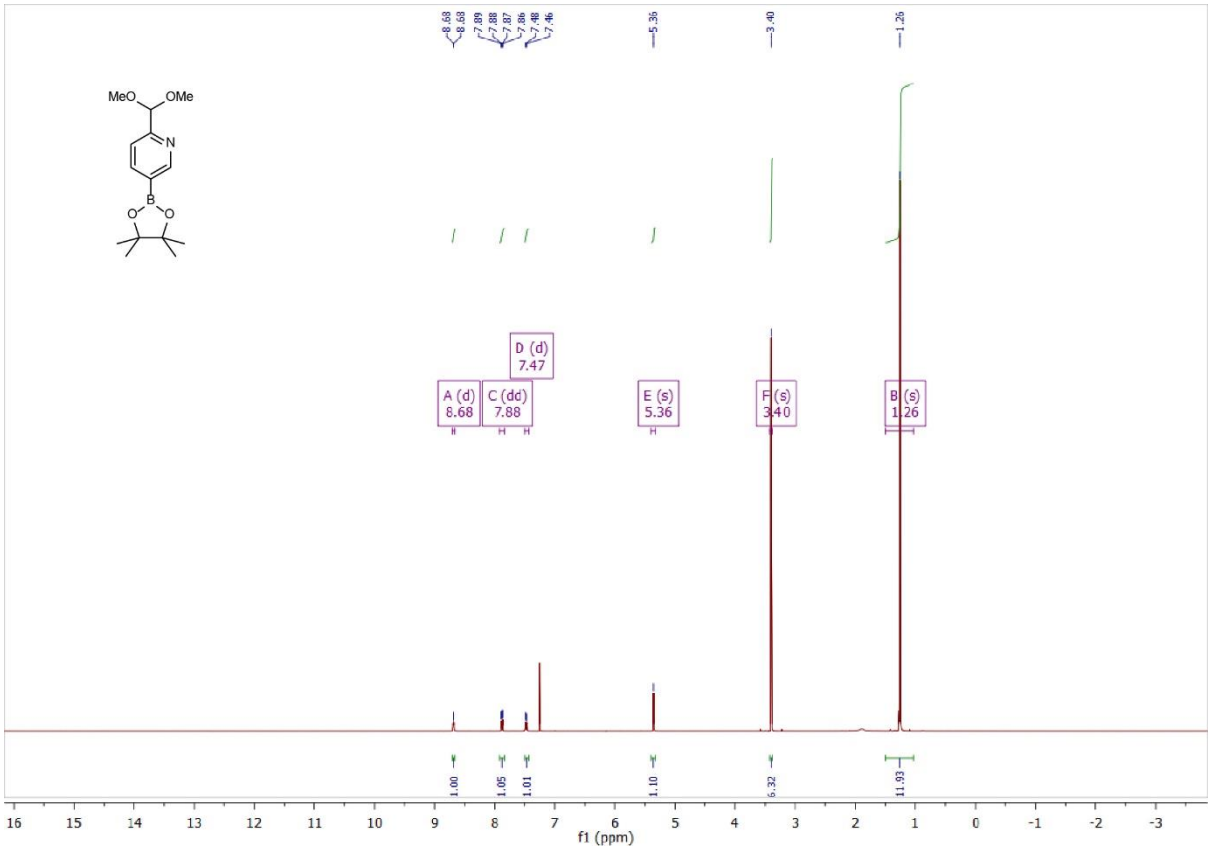

^{1}H NMR spectrum of 2-(dimethoxymethyl)-5-(4,4,5,5-tetramethyl-1,3,2-dioxaborolan-2-yl)pyridine (400 MHz, $CDCl_3$).

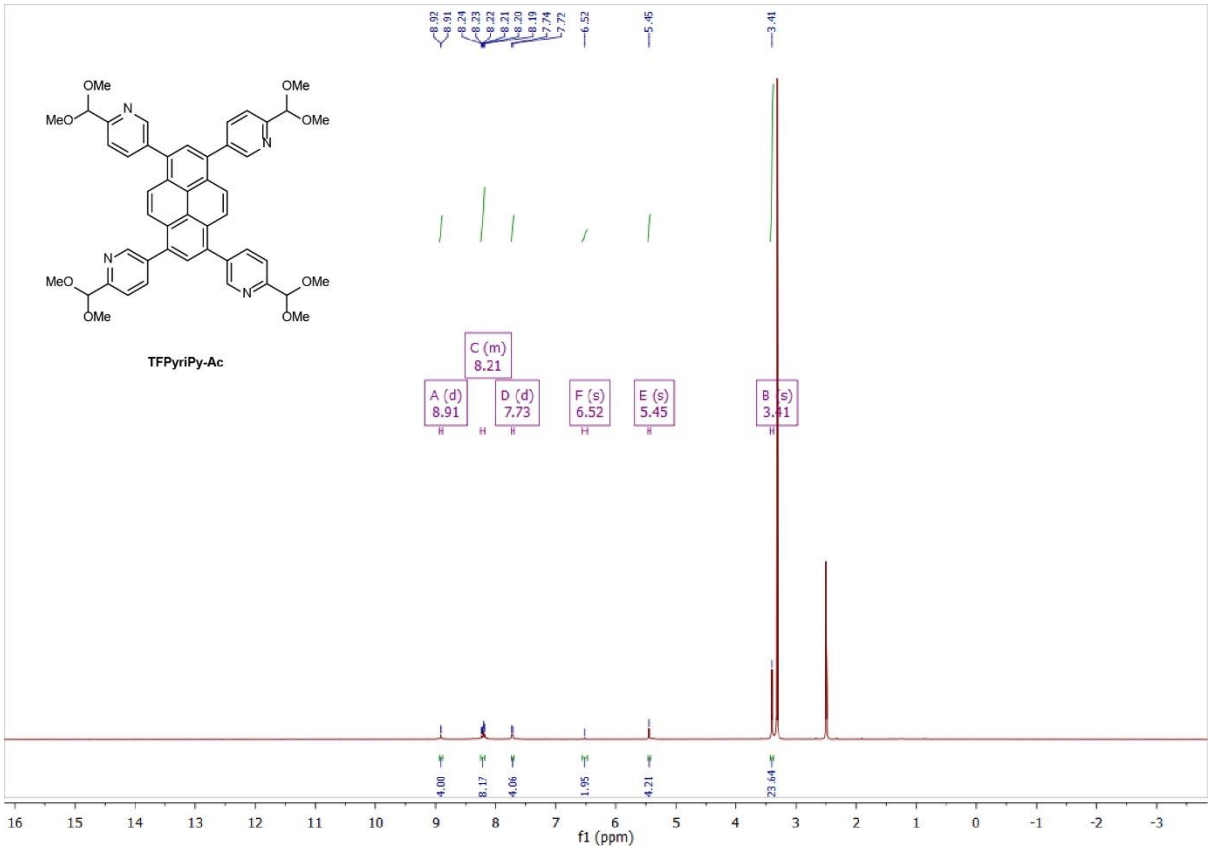

[1]H NMR spectrum of TFPyriPy-Ac (400 MHz, DMSO-*d*6).

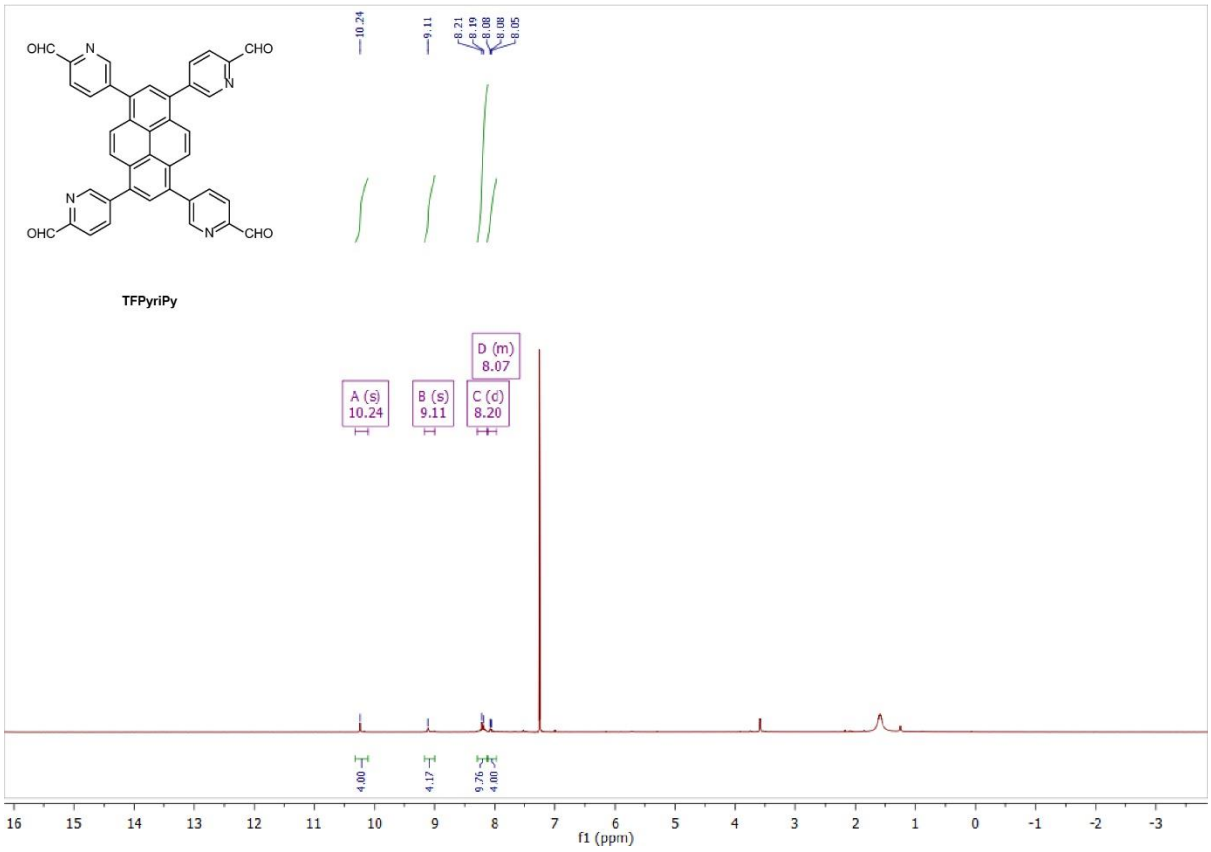

^{1}H NMR spectrum of TFPyriPy-Ac (400 MHz, $CDCl_3$).

ORTEP-style illustration of the single-crystal structures of the COF model compounds

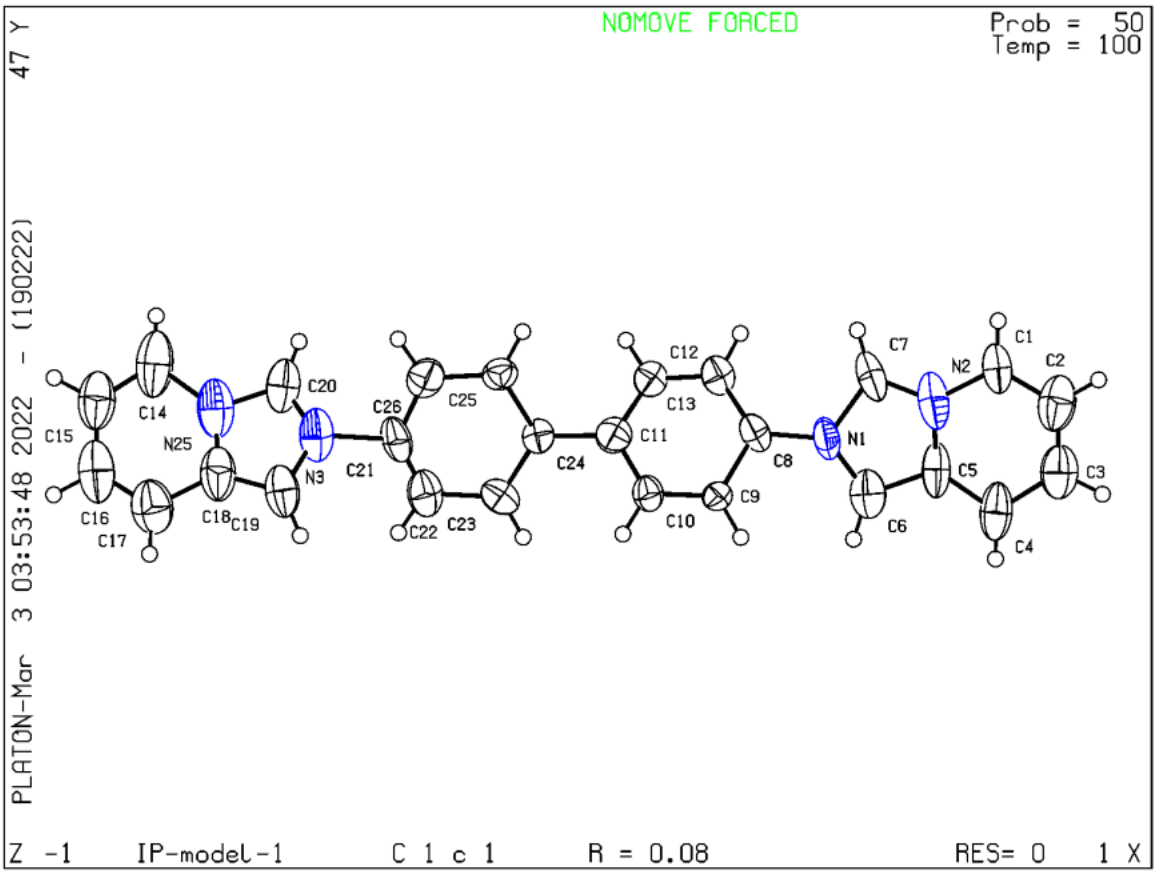

ORTEP-style illustration of IP-model-1 with CCDC deposition number of 2132342.

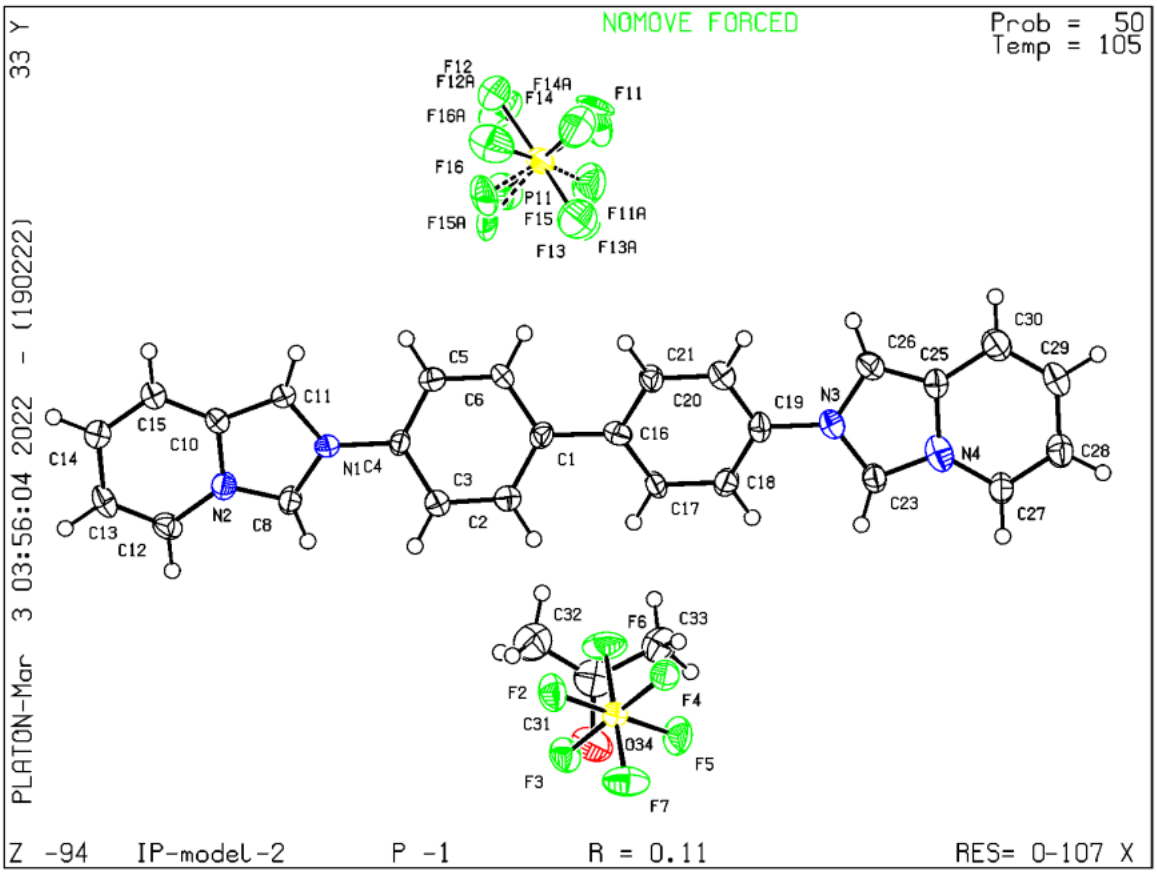

ORTEP-style illustration of IP-model-2 with CCDC deposition number of 2150060.

Fractional atomistic coordinates for the COF unit cell parameters

Supplementary Table 1 | Fractional atomistic coordinates for Pawley-refined unit cell parameters of Im-COF-1 with eclipsed stacking. Space group C2/M, a = 39.3311 Å, b = 40.5776 Å, c = 3.9055 Å, $\alpha = \gamma = 90°$, and $\beta = 110.8516°$.

	Atom	*x*	*y*	*z*
C1	C	-0.43019	0.4701	-0.54408
C2	C	-0.46511	0.46999	-0.52484
C3	C	-0.517	0.44089	-0.49088
C4	C	-0.40833	0.44023	-0.52179
C5	C	-0.4188	0.41319	-0.74218
C6	C	-0.39744	0.38604	-0.7235
C7	C	-0.36449	0.38571	-0.49473
C8	C	-0.35349	0.4129	-0.27589
C9	C	-0.37528	0.43971	-0.2888
N10	N	-0.34326	0.35756	-0.49918
C11	C	-0.31102	0.35407	-0.33575
C12	C	-0.29294	0.32374	-0.37685
N13	N	-0.31003	0.29917	-0.57937
C14	C	-0.29441	0.27083	-0.62968
C15	C	-0.25899	0.26564	-0.47174
C16	C	-0.24129	0.29125	-0.25901
C17	C	-0.25809	0.32003	-0.21197
H18	H	-0.52873	0.41732	-0.4917
H19	H	-0.44341	0.413	-0.93136
H20	H	-0.40622	0.36549	-0.89637
H21	H	-0.32855	0.41365	-0.0903
H22	H	-0.36636	0.46009	-0.1135
H23	H	-0.29673	0.37336	-0.17559
H24	H	-0.31025	0.25297	-0.79569
H25	H	-0.21443	0.28984	-0.12426
H26	H	-0.24394	0.33924	-0.04768
C27	C	-0.41405	0.5	-0.56426
C28	C	-0.48257	0.5	-0.51443
H29	H	-0.38776	0.5	-0.58988

Supplementary Table 2 | Fractional atomistic coordinates for Pawley-refined unit cell parameters of IP-COF-1 with eclipsed stacking. Space group C2/M, a = 40.8202 Å, b = 36.6902 Å, c = 4.3897 Å, $\alpha = \gamma = 90°$, and $\beta = 124.3998°$.

	Atom	*x*	*y*	*z*
C1	C	-0.4209	0.46674	-0.30061
C2	C	-0.46043	0.46652	-0.40155
C3	C	-0.51939	0.43388	-0.55058
C4	C	-0.39768	0.43337	-0.24833
C5	C	-0.40976	0.40762	-0.51953
C6	C	-0.38531	0.37916	-0.48861
C7	C	-0.34764	0.3764	-0.18882
C8	C	-0.33614	0.40146	0.08837
C9	C	-0.36082	0.42963	0.05845
N10	N	-0.32042	0.35021	-0.17769
C11	C	-0.28116	0.35245	0.01773
C12	C	-0.26661	0.32443	-0.08506
N13	N	-0.29599	0.30497	-0.33641
C14	C	-0.29147	0.27623	-0.50327
C15	C	-0.25345	0.26577	-0.40992
C16	C	-0.22215	0.28662	-0.14011
C17	C	-0.22862	0.31609	0.02385
H18	H	-0.53334	0.40776	-0.59364
H19	H	-0.43761	0.41029	-0.76121
H20	H	-0.39526	0.36081	-0.71026
H21	H	-0.30781	0.39976	0.3267
H22	H	-0.35083	0.44908	0.27268
H23	H	-0.26446	0.37361	0.20624
H24	H	-0.31712	0.26257	-0.70407
H25	H	-0.19237	0.28096	-0.05114
H26	H	-0.20473	0.33192	0.22626
C27	C	0.67143	0.67917	0.6095
C28	C	0.05289	-0.23827	-0.70336
C29	C	0.09551	-0.23795	-0.44346
O30	O	0.11676	-0.26295	-0.45037
O31	O	0.1107	-0.21276	-0.21513
F32	F	0.0369	-0.26938	-0.65659
F33	F	0.04611	-0.23792	-1.04251
F34	F	0.03561	-0.20802	-0.65746
H37	H	0.64267	0.68837	0.41541
C35	C	-0.40214	0.5	-0.25414
C36	C	-0.4802	0.5	-0.4513
H38	H	-0.37227	0.5	-0.18829

Supplementary Table 3 | Fractional atomistic coordinates for Pawley-refined unit cell parameters of Im-COF-2 with eclipsed stacking. Space group P2/M, a = 28.0757, b = 29.8356 Å, c = 3.6148 Å, $\alpha = \gamma$ = 90°, and β = 100.6911°.

	Atom	*x*	*y*	*z*
C1	C	0.04487	-0.09705	0.52965
C2	C	0.04346	-0.04861	0.5046
C3	C	0.08348	-0.02375	0.47251
C4	C	0.09285	-0.12454	0.60003
C5	C	0.14372	-0.11167	0.88735
C6	C	0.1882	-0.13761	0.95103
C7	C	0.18166	-0.17751	0.73544
N8	N	0.13202	-0.19056	0.4681
C9	C	0.08815	-0.16558	0.39817
C10	C	0.45698	-0.54849	0.50263
C11	C	0.41467	-0.47619	0.50447
C12	C	0.45762	-0.59679	0.50533
C13	C	0.41598	-0.37654	0.52108
C14	C	0.38195	-0.35366	0.53854
C15	C	0.65791	-0.32556	0.43805
C16	C	0.35517	-0.28149	0.7178
C17	C	0.31641	-0.25353	0.73398
C18	C	0.26396	-0.26965	0.59593
C19	C	0.25124	-0.3138	0.43886
C20	C	0.29011	-0.34176	0.42364
N21	N	0.22203	-0.24155	0.58878
C22	C	0.22819	-0.20442	0.78851
H23	H	0.11472	-0.04068	0.43781
H24	H	0.14911	-0.08158	1.06349
H25	H	0.22727	-0.12683	1.16864
H26	H	0.0498	-0.17757	0.1813
H27	H	0.38126	-0.45886	0.50786
H28	H	0.39523	-0.26853	0.82277
H29	H	0.32757	-0.21923	0.84554
H30	H	0.21098	-0.32646	0.32674
H31	H	0.27951	-0.37575	0.30032
H32	H	0.26729	-0.19261	0.99569
C33	C	0	-0.02436	0.5
C34	C	0	-0.12026	0.5
H35	H	0	-0.15726	0.5
C36	C	0.5	-0.52426	0.5
C37	C	0.5	-0.6203	0.5
H38	H	0.5	-0.65744	0.5

Supplementary Table 4 | Fractional atomistic coordinates for Pawley-refined unit cell parameters of IP-COF-2 with eclipsed stacking. Space group P2/M, a = 28.4561, b = 29.3199Å, c = 4.6121 Å, $\alpha = \gamma$ = 90°, and β = 107.9714°.

	Atom	*x*	*y*	*z*
C1	C	0.04785	-0.10153	0.65874
C2	C	0.04877	-0.05086	0.63852
C3	C	0.09735	-0.02485	0.74246
C4	C	0.09654	-0.12959	0.8368
C5	C	0.12925	-0.11541	1.13026
C6	C	0.17914	-0.13774	1.27949
C7	C	0.19405	-0.17511	1.13298
N8	N	0.16151	-0.18951	0.86232
C9	C	0.11317	-0.16913	0.7087
C10	C	0.46487	-0.55074	0.61254
C11	C	0.43063	-0.47511	0.72536
C12	C	0.46507	-0.60128	0.61022
C13	C	0.42885	-0.37108	0.71197
C14	C	0.39719	-0.34832	0.78743
C15	C	0.64276	-0.32172	0.13825
C16	C	0.37214	-0.28722	1.08838
C17	C	0.33244	-0.25914	1.14022
C18	C	0.27748	-0.26524	0.96524
C19	C	0.26317	-0.30173	0.74837
C20	C	0.30269	-0.32944	0.69604
N21	N	0.23681	-0.2329	0.99181
C22	C	0.24091	-0.20186	1.21763
H23	H	0.13617	-0.04256	0.81865
H24	H	0.11684	-0.08602	1.23884
H25	H	0.205	-0.12612	1.49948
H26	H	0.0895	-0.1818	0.48665
H27	H	0.40381	-0.45703	0.81733
H28	H	0.4143	-0.28124	1.21969
H29	H	0.3451	-0.23183	1.3107
H30	H	0.22143	-0.30855	0.61477
H31	H	0.29071	-0.35627	0.52118
H32	H	0.27513	-0.19843	1.42387
C33	C	0.18791	0.77561	0.77872
H34	H	0.17246	0.75817	0.56428
C35	C	1.08187	0.66114	1.70443
C36	C	1.13089	0.67695	1.95485
O37	O	1.17371	0.65193	2.03524
O38	O	1.12993	0.71611	2.08645
F39	F	1.09175	0.61885	1.58204
F40	F	1.03982	0.6544	1.80882
F41	F	1.06733	0.69626	1.48693
C42	C	0	-0.02548	0.5

C43	C	0	-0.12609	0.5
H44	H	0	-0.16489	0.5
C45	C	0.5	-0.52539	0.5
C46	C	0.5	-0.6259	0.5
H47	H	0.5	-0.66472	0.5

Summary of representative cathode materials for enhanced Li-S battery performance.

Supplementary Table 5 | A summary of representative cathode materials for enhanced Li-S battery performance.

Strategy	Materials	Materials loading (wt%)	Low-loading cathode (Areal capacity < 3 mAh cm^{-2})		High-loading cathode (Areal capacity > 3.5 mAh cm^{-2})		Ref.
			Capacity fading (cycle number)	Rate capability (C rate)	Areal capacity (mAh cm^{-2})	Capacity fading (cycle number)	
Chemically Ambivalent Framework	**IP-COF-1**	**4%**	**0.041% (600)**	**630 mAh g^{-1} (5 C)** **540 mAh g^{-1} (10 C)**	**6.2**	**0% (~100)**	**This work**
COF-based host	CTF-1	15%	0.047% (300)	401 mAh g^{-1} (2 C)	-	-	2
	COF-1	36%	0.13% (200)	620 mAh g^{-1} (1 C)	-	-	3
	PI-CON (exfoliated)	21%	0.025% (500)	620 mAh g^{-1} (4 C)	-	-	4
COF-based binder	OH-AAn COF	1%	0.125% (300)	515.7 mAh g^{-1} (2 C)	4	0.3% (100)	5
Porous organic polymer (POP)-based host	POF-HS	-	0.095% (200)	800 mAh g^{-1} (4 C)	-	-	6
MOF-based host	HKUST-1	18%	0.08% (500)	449 mAh g^{-1} (10 C)	7.45	~0.23% (50)	7
Redox-active additive	Mo_6S_8	42.5%	-	-	7.8	0.17% (100)	8
	HATN	16%	0.029% (1000)	-	10.5	0.1% (200)	9
	AQ	18%	0.07% (500)	427.4 mAh g^{-1} (2 C)	-	-	10
Single-atom catalyst	ZnS, Co-N-C	20%	-	700 mAh g^{-1} (5 C)	7.49	0.13% (100)	11
	Co atom	0.06%	0.053% (500)	618 mAh g^{-1} (5 C)	5.1	0.029% (100)	12
Electrocatalyst	MgB_2	16%	0.04% (200)	-	6.18	~0.34% (100)	13

References

1 Dassault Systèmes BIOVIA, Materials Studio, Version 2016, San Diego: Dassault Systèmes (2017).

2 Talapaneni, S. N. *et al.* Elemental-Sulfur-Mediated Facile Synthesis of a Covalent Triazine Framework for High-Performance Lithium–Sulfur Batteries. *Angew. Chem., Int. Ed.* **55,** 3106-3111 (2016).

3 Ghazi ZA, *et al.* Efficient Polysulfide Chemisorption in Covalent Organic Frameworks for High-Performance Lithium-Sulfur Batteries. *Adv. Energy Mater*. **6**, 1601250 (2016).

4 Duan, H. *et al.* Scalable Synthesis of Ultrathin Polyimide Covalent Organic Framework Nanosheets for High-Performance Lithium–Sulfur Batteries. *J. Am. Chem. Soc.* **143,** 19446-19453 (2021).

5 Guo C, *et al.* Anthraquinone Covalent Organic Framework Hollow Tubes as Binder Microadditives in Li−S Batteries. *Angew. Chem., Int. Ed.* (2021), https://doi.org/10.1002/anie.202113315.

6 Li, B.-Q., Zhang, S.-Y., Kong, L., Peng, H.-J. & Zhang, Q. Porphyrin Organic Framework Hollow Spheres and Their Applications in Lithium–Sulfur Batteries. *Adv. Mater*. **30,** 1707483 (2018).

7 Mao Y, *et al.* Foldable interpenetrated metal-organic frameworks/carbon nanotubes thin film for lithium–sulfur batteries. *Nat. Commun.* **8**, 14628 (2017).

8 Xue W, *et al.* Intercalation-conversion hybrid cathodes enabling Li–S full-cell architectures with jointly superior gravimetric and volumetric energy densities. *Nat. Energy* **4**, 374-382 (2019).

9 Wang X, *et al.* Dense-Stacking Porous Conjugated Polymer as Reactive-Type Host for High-Performance Lithium Sulfur Batteries. *Angew. Chem., Int. Ed.* **60**, 11359-11369 (2021).

10 Li G, *et al.* Chemisorption of polysulfides through redox reactions with organic molecules for lithium–sulfur batteries. *Nat. Commun.* **9**, 705 (2018).

11 Zhao C, *et al.* A high-energy and long-cycling lithium–sulfur pouch cell via a macroporous catalytic cathode with double-end binding sites. *Nature Nanotechnology* **16**, 166-173 (2021).

12 Du Z, *et al.* Cobalt in Nitrogen-Doped Graphene as Single-Atom Catalyst for High-Sulfur Content Lithium–Sulfur Batteries. *J. Am. Chem. Soc.* **141**, 3977-3985 (2019).

13 Pang Q, Kwok CY, Kundu D, Liang X, Nazar LF. Lightweight Metallic MgB2 Mediates Polysulfide Redox and Promises High-Energy-Density Lithium-Sulfur Batteries. *Joule* **3**, 136-148 (2019).